Structure and Dynamics of Water-Smectite Interfaces: Hydrogen Bonding and the Origin of the Sharp O-Dw/O-Hw Infrared Band From Molecular Simulations

Marek Szczerba, Artur Kuligiewicz, Arkadiusz Derkowski, Vassilis Gionis, Georgios D. Chryssikos, Andrey G. Kalinichev

Marek Szczerba, Artur Kuligiewicz, Arkadiusz Derkowski, Vassilis Gionis, Georgios D. Chryssikos, et al.. Structure and Dynamics of Water-Smectite Interfaces: Hydrogen Bonding and the Origin of the Sharp O-Dw/O-Hw Infrared Band From Molecular Simulations. Clays and Clay Minerals, 2016, 64 (4), pp.452-471. 10.1346/ccmn.2016.0640409 . in2p3-01577621

HAL Id: in2p3-01577621
https://hal.in2p3.fr/in2p3-01577621

Submitted on 9 Oct 2018

Structure and dynamics of water-smectite interfaces: Hydrogen bonding and the origin of the sharp O-D$_w$/O-H$_w$ infrared band from molecular simulations

Marek Szczerba[1,*], Artur Kuligiewicz[1], Arkadiusz Derkowski[1],
Vassilis Gionis[2], Georgios D. Chryssikos[2],
Andrey G. Kalinichev[3]

[1] Institute of Geological Sciences, Polish Academy of Sciences, Krakow, Poland

[2] Theoretical and Physical Chemistry Institute, National Hellenic Research Foundation, Athens, Greece

[3] Laboratoire SUBATECH (UMR 6457), Ecole des Mines de Nantes, Nantes, France

*) Corresponding author: ndszczer@cyf-kr.edu.pl

KEY WORDS: clay-water interface, adsorbed water, smectite, molecular dynamics, infrared spectroscopy

ABSTRACT

Experimental studies have shown that a sharp high-frequency IR band at ~3615 cm^{-1} (in H_2O form) and at ~2685 cm^{-1} (in D_2O form) is a common feature for all smectites, and its position correlates with layer charge. In order to explain the molecular origin of this band in terms of total layer charge, charge localization, as well as nature of interlayer cations influencing the position and intensity of this peak, a series of classical MD simulations were performed for several smectite models. The smectite layers were described using a modified CLAYFF force field, where the intramolecular vibrations of H_2O were more accurately described by the Toukan-Rahman potential. The power spectra of molecular vibrations of hydrogens were calculated for selected sub-sets of interlayer H_2O to quantitatively analyze their contribution to the observed spectral features. The statistics of hydrogen bonds in the smectite interlayers were also analyzed to support the spectral calculations.

The simulation results demonstrated clearly that only the H_2O molecules in close proximity with the smectite surface are responsible for the observed sharp vibrational band. Other hypotheses on the possible origins of this band were carefully considered and eventually rejected. Two orientations of H_2O molecules donating one or two H-bonds to the basal oxygens of the smectite surface (monodentate and bidentate orientations, respectively) are observed. In both orientations these H-bonds are quite weak, pointing to a generally hydrophobic character of the smectite surface. Both orientations were found to contribute to the high-frequency band, but the monodentate orientation provides the predominant contribution because surface H_2O molecules in this orientation are much more abundant. In good agreement with experiment, only a small difference in the peak position was observed between smectites with different charge localization. The effect of the total layer charge, i.e. the red-shift for higher charge smectites, was also confirmed. This shift arises from the decrease of the H-bonding distances of H_2O in monodentate and bidentate orientation.

INTRODUCTION

Fourier transform infrared spectroscopy (FTIR) is one of the most commonly used techniques for studying clay minerals. However, unambiguous assignment of the vibrational bands originating from the stretching modes of adsorbed molecular H_2O (O-H_w) and structural OH (O-H_s) in the clay materials is not always feasible. This is especially true for swelling clay minerals like smectites, which have large water sorption capacities (e.g., Cases *et al.*, 1997; Sato *et al.*, 1992) and may contain significant amounts of adsorbed water under air-dry conditions even upon prolonged drying (e.g., Środoń and McCarty, 2008).

Kuligiewicz *et al.* (2015a) have recently presented new evidence that the sharp high-frequency bands observed at ~3610-3640 cm^{-1} involve a significant contribution from weakly hydrogen-bonded O-H_w of adsorbed H_2O molecules. These observations were in agreement with earlier spectroscopic measurements (Russell and Farmer, 1964; Farmer and Russell, 1971; Suquet *et al.*, 1977; Sposito and Prost, 1982; Cariati *et al.*, 1981, 1983; Sposito *et al.*, 1983), and opened the possibility for obtaining layer charge diagnostics based on the vibrational signature of H_2O in smectite (Kuligiewicz *et al.*, 2015b).

Early computational molecular modeling studies of clays (Skipper *et al.*, 1991; Chang *et al.*, 1995; Boek *et al.*, 1995; Greathouse and Sposito, 1998; Sposito *et al.*, 1999) suggested the existence of H-bonds between water and siloxane surfaces. This H-bonding implies a specific spatial arrangement of the surface H_2O molecules with respect to oxygen atoms of the basal plane. These MD calculations confirmed the model of Prost (1975) with one O-H_w bond of the H_2O molecule directed towards the clay surface, donating an H-bond to the basal oxygen atom.

The existence of such interfacial H-bonding with one O-H_w bond oriented towards the clay surface was later confirmed by simulations of smectites and muscovite (e.g. Wang *et al.*, 2005b, 2009; Marry *et al.*, 2008, 2013; Morrow *et al.*, 2013; Ngouana Wakou and Kalinichev, 2014; Greathouse *et al.,* 2015; Teich-McGoldrick *et al.,* 2015; Zaunbrecher *et al.,* 2015, Loganathan *et al.*, 2016a, 2016b), using more sophisticated force fields, specifically optimized for clay mineral studies, such as CLAYFF (Cygan *et al.*, 2004). The existence of an additional type of interfacial H_2O located above the ditrigonal cavities of smecites and with both O-H_w bonds directed towards the basal surface was also reported for 2:1 sheet silicates of high total layer charge (Wang *et al.*, 2005b, 2009). *Ab-initio* calculations showed that these H-bonds are relatively short-lived and weaker than typical $H_2O \cdots H_2O$ in liquid water (Boek and Sprik, 2003).

In addition, Suzuki and Kawamura (2004) calculated the theoretical FTIR spectra of water adsorbed on Na-beidellite with total layer charge of 0.33 per half unit cell (phuc). Based on their modeling, the O-H_w bonds pointing towards the surface of beidellite contribute to a vibrational band at ~3500 cm^{-1}, whereas the O-H_w H-bonded to other H_2O molecules produce a band at ~3365 cm^{-1}. The relative intensity of the ~3365 to the ~3500 cm^{-1} bands increased with increasing water content, and for 7 H_2O molecules phuc the band at ~3500 cm^{-1} was no longer detectable.

The experimental and theoretical evidence of the hydrophobic character of the siloxane surface of uncharged clays has been broadly discussed in the literature (e.g., Michot et al., 1994, Bridgeman and Skipper, 1997; Arab et al., 2003; Tunega et al., 2004; Wang et al., 2004; 2005a; Churakov, 2006; Rotenberg et al., 2011; Šolc et al., 2011).However, for the siloxane surface of charged clays, like smectites, the picture is not as clear. Based on aromatic hydrocarbon adsorption experiments, Jaynes and Boyd (1991) have classified this surface as mostly hydrophobic. On the other hand, Sobolev et al. (2010) have used neutron scattering technique to determine that the surfaces of smectite clays with tetrahedral substitutions are hydrophilic. The importance of the specific structural charge location within a clay layer for the existence of hydrophobic and hydrophilic patches on its surface has also been determined in Monte Carlo computer simulations (Sposito et al., 1999). The relative weakness of the H-bonds donated by the interlayer water molecules to the clay basal surface, compared to the typical strength of the $H_2O\cdots H_2O$ bonds in bulk liquid water can be considered as a molecular-scale indication of relative hydrophobicity of the smectite siloxane surface.

The present study is aimed at advancing the aforementioned discussion by adding new spectroscopic arguments. Vibrational spectra of interfacial water molecules in several smectites are calculated and carefully analyzed here on the basis of molecular dynamics simulations in order to identify, interpret and quantify the variability of the position of the sharp H_2O vibrational band as a function of total clay layer charge, layer charge localization, and nature of the interlayer cations, as recently observed experimentally (Kuligiewicz *et al.,* 2015a).

METHODOLOGY

Smectite structures and MD simulations

In order to explore systematically the effects of smectite composition, type of the interlayer cations and water content on the structure of interlayer H_2O, a series of MD simulations were performed on four models of dioctahedral smectites with a total layer charge of 0.3 or 0.5 phuc and octahedral (montmorillonitic) or tetrahedral (beidellitic) charge localization:

Beid03: $M^{+}_{0.3}(Al_{2.0})(Si_{3.7}Al_{0.3})O_{10}(OH)_2$;

Beid05: $M^{+}_{0.5}(Al_{2.0})(Si_{3.5}Al_{0.5})O_{10}(OH)_2$;

Mtm03: $M^{+}_{0.3}(Al_{1.7}\,Mg_{0.3})(Si_{4.0})O_{10}(OH)_2$;

Mtm05: $M^{+}_{0.5}(Al_{1.5}\,Mg_{0.5})(Si_{4.0})O_{10}(OH)_2$.

The interlayer water content (2.5, 5.0 and 7.5 H_2O phuc) and the type of the interlayer cation

(Na^+, Cs^+, and Ca^{2+}) for selected water contents were used as additional variables.

The structural models of the smectites were built on the basis of the pyrophyllite crystal structure (Lee and Guggenheim, 1981), with isomorphic substitutions introduced at specific atomic sites. The Mg/Al ordering in the octahedral sheets was set by maximizing the distance between Mg atoms, following the work of Ortega-Castro *et al.* (2010). The Al/Si ordering in the tetrahedral sheet was random but following the Löwenstein rule, *i.e.* excluding Al-O-Al linkages (Löwenstein, 1954). The simulation supercell was 8×4×2 unit cells in the *a*, *b*, and *c* crystallographic directions, respectively (~41.6 Å × 36.1 Å × Z Å; the value of Z varied in the ~12.5-19.0 Å range depending mainly on the amount of water in the interlayer space). The edge surfaces were not considered.

The atoms of the smectite structure were not fixed – i.e. they were allowed to move around their crystallographically determined positions according to the modeling force field used. Only one cation in one octahedral sheet was kept frozen in its position in order to keep 2:1 layers in place during the entire simulation span. Partial atomic charges and other interatomic interaction parameters of smectite layers were described using the CLAYFF force field (Cygan *et al.*, 2004) with structural OH groups modified by introducing a more accurate Morse potential (Greathouse *et al.*, 2009). Ewald summation was used to calculate the long range corrections to the electrostatic interactions and the cutoff distance was set at 10.0 Å. Non-electrostatic Lennard-Jones parameters of the interatomic interactions involving bridging oxygen atoms were modified after Ferrage *et al.* (2011) in order to improve the description of the interlayer water structure of hydrated smectites. The necessity of this modification was justified based on comparisons of experimental and calculated XRD and neutron diffraction data (Ferrage *et al.*, 2011). However, unlike the original suggestion of Ferrage *et al.* (2011), only the parameters of surface oxygen atoms were modified in our work, because initial test simulations showed that the modification for all bridging oxygen atoms leads to a substantial and unrealistic deformation of the clay octahedral sheet if the cell volume is not constrained in the simulations at constant pressure, i.e., in the *NPT* statistical ensemble (see Supplementary materials). Additionally, the Lennard-Jones parameters of tetrahedral Si and tetrahedral Al in the clay structure were also modified to compensate for the increased size of the surface bridging oxygen atoms by applying the usual arithmetic mixing rules for the parameters of interatomic interactions (Table 1).

=== Table 1 ===

For a more accurate description of the vibrational properties of water molecules, the parameters of intramolecular interactions for H_2O were taken from the work of Toukan and Rahman (1985) using the implementation proposed by Praprotnik *et al.* (2004). This allowed a more accurate description of the anharmonicity of the O_w-H_w stretching vibrations in the calculated IR spectra in comparison to the simple harmonic vibrational terms of the original CLAYFF parameterization (Cygan *et al.*, 2004).

NPT-ensemble MD simulations at constant pressure (P = 1 bar) and temperature (T = 300 K) were performed for 2.0 ns with the time step of 1 fs, preceded by one temperature annealing cycle from 400 K to 300 K of 0.1 ns. This long equilibration run was followed by a short 10 ps data analysis run when atomic positions and velocities were recorded every 2 fs. Standard periodic boundary conditions were applied (e.g., Allen and Tildesley, 1987) and all simulations were performed using the LAMMPS molecular modeling program (Plimpton, 1995).

Simulation analysis

The MD-simulated structural data were used to calculate the distributions of angles formed by the dipole axis of interfacial H_2O molecules with respect to a vector normal to the 2:1 surfaces (angle α) as a function of the distance z of O_w from the plane of the basal bridging oxygens (O_b). The direction of the H_2O dipole was defined as a vector from the oxygen atom O_w to the central point between the two hydrogen atoms H_w of the same molecule. As the HOH angle was allowed to vary in the flexible H_2O molecular model used, this methodology introduces some small additional spread of the calculated angles. Additionally, the distributions of angles between a given OH bonds of H_2O and a vector normal to the 2:1 surfaces were calculated as a function of the distance z from the O_b plane (angle β). The position of the plane of basal oxygen atoms was determined by the maximum of the atomic density distribution for these atoms, similarly to the previous studies (Wang *et al.,* 2005b, 2009; Loganathan and Kalinichev, 2013; Szczerba *et al.*, 2014, Ngouana Wakou and Kalinichev, 2014; Greathouse *et al.*, 2015; Teich-McGoldrick *et al.*, 2015 ; Loganathan *et al.*, 2016a, 2016b). All these properties were calculated by averaging over the last 1 ns of the equilibrium MD simulation runs.

Calculation of power spectra

MD-simulated atomic trajectories can be used to calculate so-called power spectra (PS) of atomic vibrations that contain an entire distribution of the power (density of states) of all atomic motions in the simulated system in a function of vibrations frequency. With certain restrictions, these power spectra can be compared to the experimental vibrational spectra (e.g., Allen and Tildesley, 1987; Kleinhesselink and Wolfsberg 1992). The power spectra are obtained as Fourier transformations of the so-called velocity autocorrelation function (VACF), which, in turn, can be directly calculated from the MD-simulated dynamic trajectories of the atoms in the modeled system. The frequency of H_2O stretching vibration is usually well captured by the VACF of the water hydrogen atoms (e.g., Kalinichev, 2001).

In the present work, normalized VACF based on the last 10 ps period of every MD simulation run were calculated for selected hydrogen atoms with a moving window of 1 ps from the equilibrium part of the MD trajectory recorded every 2 fs:

$$\mathrm{VACF}(t) = \frac{\sum_{f=1}^{n-n_{\mathrm{VACF}}} \sum_{\mathrm{sel.atoms}} \vec{v}_f \cdot \vec{v}_{f+t}}{\sum_{f=1}^{n-n_{\mathrm{VACF}}} \sum_{\mathrm{sel.atoms}} \vec{v}_f \cdot \vec{v}_f}; \qquad (2)$$

where n - is the total number of windows, n_{VACF} - is the number of windows used in a particular calculation of VACF. The first sum in nominator and denominator corresponds to averaging over total number of windows minus the number of VACF windows. The second sum is calculated over all hydrogen atoms of water molecules, or their selected subset based on the distance of the respective H_2O from the clay surface and the angle of H_2O dipole orientation (or angle between one of OH groups of H_2O and a vector normal to the 2:1 surface). The scalar products of instantaneous atomic velocities and their subsequent Fourier transformation into vibrational power spectra were calculated according to standard VACF and PS definitions (e.g., Allen and Tildesley, 1987; Kleinhesselink and Wolfsberg, 1992). For every VACF window, the determination of a H_2O molecule as belonging to a selected position/orientation population was checked at the beginning and at the end of the VACF window. The chosen short duration of the analysis run (10 ps) is, nevertheless, long enough in respect to a typical H-bonding lifetime (0.8-0.9 ps; Kumar *et al.*, 2007), but still short enough not to allow H_2O to change significantly their positions in the interlayer with respect to the clay surface. At the same time, the relatively short time of the individual VACF window (1 ps) is comparable with a typical H-bonding lifetime, but still allows to probe the stretching dynamics of the selected O-H_w bonds (e.g., Kalinichev, 2001). The choice of both characteristic calculation times ensured that the H-bonding situation of each H_2O molecule was included in a certain selected angle/position subset for VACF calculation.

In order to calculate the power spectra of H_2O vibrations, a cosine Fourier transform of VACF for the water hydrogen atoms was performed as:

$$\mathrm{PS}(\omega) = \sum_{t=1}^{n_{\mathrm{VACF}}} \mathrm{VACF}(t) \cdot \cos\left(\frac{\pi}{n_{\mathrm{VACF}}} \cdot t \cdot \omega\right) \tag{3}$$

The statistical noise was preliminarily reduced by applying a filtering function:

$$\mathrm{VACF}(t) = \mathrm{VACF}(t) \cdot \exp(-t/\tau) \tag{4}$$

where τ was set to 0.25 ps.

Due to the normalization of VACF, the intensity of the calculated power spectra can, therefore, be considered as proportional to the total number of H_2O molecules selected for each calculation.

RESULTS AND DISCUSSION

Characteristic features of MD simulations

The composition and adsorbed water content of all simulated clay models are presented in Table 2 along with the resulting basal spacings. The 2W model for Cs-smectite is purely hypothetical and does not correspond to any experimental or natural conditions (e.g., Ngouana Wakou and Kalinichev, 2014).

=== Table 2 ===

The values of the calculated basal spacings closely match those obtained by modelling the experimental diffractograms: d_{001_1W} = 11.6–12.9 Å, d_{001_2W} = 14.9–15.7 Å and d_{001_3W} = 18–19 Å (e.g., Dazas *et al.*, 2015). The data show clearly that for the same water content and interlayer cation (Na^+) the basal spacing d_{001} decreases with increasing layer charge (e.g. 15.95 Å for Mtm03Na_2W and 15.37 Å for Mtm05Na_2W). This trend is in agreement with literature data (e.g., Sato *et al.*, 1992, Ferrage *et al.*, 2005, 2007), whereas some variation is related also to the layer charge location. Substantial differences in basal spacings were also observed as a result of the replacement of interlayer cations from Na^+ or Ca^{2+} to Cs^+ (e.g., 15.37 Å for Mtm05Na_2W, 15.38 Å for Mtm05Ca_2W and 16.14 Å for Mtm05Cs_2W). These differences were caused mainly by the increased size of the cation and by differences in hydration energies.

In agreement with other recent simulations (e.g. Wang *et al.*, 2005b, 2009; Morrow *et al.*, 2013; Ngouana Wakou and Kalinichev, 2014; Greathouse *et al.*, 2015; Teich-McGoldrick *et al.*, 2015; Zaunbrecher *et al.*, 2015; Loganathan *et al.*, 2016a, 2016b), a typical snapshot of the interlayer structure (Figure 1) illustrated that H_2O molecules close to the siloxane surface tend to be specifically oriented. Within a distance of < 3.5 Å between O_w and the siloxane surface two such preferred orientations could be distinguished. The population closer to the surface corresponds to H_2O with both O-H_w bonds pointing towards the surface (bidentate), whereas a more distant and more pronounced population is due to the H_2O pointing only one of their O-H_w bonds towards the surface and the second one towards the bulk of the interlayer (monodentate). In order to quantify these differences, these two populations were investigated as a function of smectite charge, type of the interlayer cations, and degree of hydration.

=== Figure 1 ===

Position of the cations in the interlayer space

The distribution of interlayer cations for different smectites (blue solid lines in Figures 2 and 3) exhibited a clear dependence on the amount and location of layer charge, as well as on the type of the cation. In the case of 1W sodium smectites, two separate maxima were visible, each corresponding to inner-sphere coordination of H_2O to the surface. For 2W sodium structures, a strong tendency to form a third maximum corresponding to fully hydrated cations (outer sphere) in the middle of the interlayer was observed. The ratio between the central and wing (inner sphere) cation distributions depended on the charge location, whereas changes in total charge had similar effect on both of these maxima. This result is in agreement with other recent simulations and is supported by calculated XRD data (Dazas *et al.,* 2015; Teich-McGoldrick *et al.,* 2015). In the case of 3W structures, outer-sphere sodium ions formed two maxima close to the interlayer center instead of one as in 2W. The data for the Mtm03Na_3W structure were very similar to the results presented by Dazas *et al.* (2014). With increasing tetrahedral charge a tendency to form higher amount of inner-sphere complexes with the siloxane surface was observed.

The effect of changing interlayer cation from Na^+ to Ca^{2+} was investigated for the models with 2W hydration. Comparison of smectites in Ca^{2+} form (Figure 3) with those in Na^+ form (Figure 2) indicated that, despite the two-fold increase in the cation hydration enthalpy, the only effect was the vanishing of the (already weak) population of cations in the vicinity of the surface. The only exception was Beid05Ca_2W, for which some remaining contribution of ions forming inner-sphere complexes was observed.

=== Figure 2 ===

=== Figure 3 ===

Oppositely, the lowest hydration enthalpy Cs^+ ions had a tendency to remain close to the surface (Figure 3), which is in excellent agreement with other recent Cs^+-smectite simulations (Ngouana Wakou and Kalinichev, 2014; Teich-McGoldrich *et al.*, 2015; Zaunbrecher *et al.*, 2015; Loganathan *et al.*, 2016a). The distribution of Cs^+ in the interlayer was substantially different from those of Na^+ and Ca^{2+}, which were generally quite similar to each other (compare Figures 2 and 3).

H_2O orientation

The contour maps of the angular distributions of the interlayer H_2O dipole vectors with respect to the direction normal to the surface (α angle) plotted in a function of the distance z from the surface (Figure 2) enabled the distinction of the two preferred surface-oriented types of water molecules marked in Figure 1. The predominantly bidentate population was located closer to the surface at $z \sim 2.0$ Å and $\alpha \sim 0$-30°, similarly to ideal theoretical values (observed in smectites with charge 0.5). A more distant and more pronounced monodentate population was at distances $z \sim 2.8$ Å and oriented in a broad range of angles between 30° and 80° with a maximum at $\alpha \sim 55$°, which matches the ideal theoretical value for one OH vector pointing perpendicularly to the smectite surface (half of the 105° angle of H_2O). For higher hydration levels, a third population of water molecules was observed closer to the middle of the interlayer. The orientational distribution of this population depended significantly on both, the hydration level of the specific smectite and the type of the interlayer cation. The latter dependence is observed clearly when comparing the distribution in Mtm05 for the same hydration levels but different interlayer cations (Figures 2 and 3).

The presence of monodentate H_2O was ubiquitous. This sub-population was abundantly visible for all smectites, all cations and all hydration levels. A noticeable dependence of the location of the distribution maxima was however observed: higher average H_2O dipole vector angles were observed for low charge smectites, lower hydration levels, and for Cs^+ as interlayer cation.

The bidentate H_2O population was far less abundant. It could be detected only in high charge smectites and was practically absent in their low charge analogs. Layer charge increasing beyond 0.5 phuc is therefore expected increase further the amount of bidentate molecules, predicting its high contribution at charges approaching 1 phuc (mica, vermiculite), which was indeed reported by Wang *et al.* (2005b, 2009) and Loganathan and Kalinichev (2013) on muscovite. Further, in all smectites studied, a dependence of the bidentate H_2O population on hydration level was observed: for a given smectite, the relative number of bidentate H_2O decreases upon drying.

The H_2O orientation also depends on the type of the interlayer cation. As the majority of Cs^+ cations are located close to smectite surface, a noticeable decrease of bidentate H_2O population in Cs^+-smectites in comparison to their Na^+- and Ca^{2+}-analogs was observed. This effect was, however, small compared to the dependence of the bidentate population on layer charge. A noticeable decrease of the maximum amplitude corresponding to monodentate population was additionally observed for the Cs^+ form. This decrease was accompanied by the transfer of H_2O to the middle of the interlayer.

Vibrational spectra of H_2O in the smectite interlayer

Kuligiewicz *et al.* (2015a, 2015b) found that the sharp high-frequency IR band originating from adsorbed water at ~3615 cm^{-1} (in H_2O form) and ~2685 cm^{-1} (in D_2O form) is a common feature for all hydrated smectites. Its intensity depended very little on the degree of clay hydration over a broad range of relative humidity, and its frequency exhibited a weak but systematic decrease (red-shift) upon increasing the total layer charge, with no measurable dependence on charge location. For a given layer charge, the dependence of the peak position on the field strength of the interlayer cation for high hydration enthalpy cations (Na^+, Ca^{2+},

Mg^{2+}) was negligible and only low hydration cations (Cs^+ , K^+) could be distinguished. These trends were opposite to what was observed for the main O-H_w (O-D_w) stretching envelopes, located at ~3400 cm^{-1} (~2500 cm^{-1}). The latter envelopes were known to exhibit a strong dependence of their intensity on hydration level and their position on interlayer cation, but were relatively unaffected by the smectite layer charge or charge localization (e.g., Xu *et al.*, 2000, Madejová *et al.*, 2002, Kuligiewicz *et al.*, 2015a, 2015b).

Thus, the sharp high-frequency IR band observed in water vapor-saturated smectites was attributed to a mechanism that must be common to all smectites at high hydration levels, regardless of interlayer cation. In addition, the high-frequency band must account for H-bonding interactions that are considerably weaker than those encountered in bulk H_2O or aqueous solutions of common salts, and its exact position ought to show a measurable dependence on the total charge of the 2:1 layer (Kuligiewicz *et al.*, 2015a, 2015b).

In order to provide a quantitative explanation for the aforementioned experimental phenomenology, the power spectra for hydrogen atoms of interlayer H_2O molecules were calculated for different smectites and compared to the spectrum of pure bulk water, the latter calculated with the same molecular model (Figure 4).

=== Figure 4 ===

The results showed that water in smectites exhibits a considerable increase of its spectral density at higher frequencies (~3600-3800 cm^{-1}) in respect to bulk water spectrum. The simulated spectrum of bulk water, however, shows some excessive high-frequency spectral density around 3730 cm^{-1}, which is not observed experimentally, and indicates some limitations of the present model. Nevertheless, the shape of the power spectrum of bulk water agrees perfectly well with the spectrum obtained earlier by the same methodology (Tay and Bresme, 2006) and still represents one of the most accurate models describing the dynamics of O_w-H_w stretching vibrations in water (e.g., Kalinichev, 2001; Guillot, 2002). Additionally, the calculated results do not show the low-frequency band at ~3250 cm^{-1}, which has been found in experimental data thus is consistent with an assignment of this band to Fermi resonance (Efimov and Naberukhin, 2002; Sovago *et al.*, 2009).

Power spectra were also calculated for four different smectites with varying content of adsorbed water: Beid03Na, Beid05Na, Mtm03Na and Mtm05Na (Figure 5). The results showed that with increasing number of H_2O molecules in the smectite interlayer the relative intensity of the lower-frequency peak at ~3500 cm^{-1} increased. This was in qualitative agreement with the experimental observations of Kuligiewicz *et al.* (2015a), who reported that the higher-frequency peak is nearly fixed and the intensity of the lower-frequency peak is greatly varying with water content. In the present study, the peak intensity at ~3750 cm^{-1} was found to depend on hydration, but this can be to some extent related to the limitations of the specific H_2O molecular models used.

=== Figure 5 ===

In order to further analyze the influence of different factors on the higher-frequency band, its positions was determined by fitting procedures. The low-frequency band was fitted with a mixed Gauss-Lorentz function (percentage of Lorentz function was optimized), while the higher-frequency one with a simple Gauss function. Additionally, a small combination band at ~ 4000 cm^{-1} was fitted with another Gaussian (Figure 6).

=== Figure 6 ===

Increasing smectite total layer charge was found to induce a noticeable red-shift of the high-frequency peak, in remarkable agreement with experiment data (Kuligiewicz et al., 2015b). This shift was observed in Na$^+$ montmorillonites and beidellites at any hydration level (Figure 7a) and also in the 2W forms for any cation (Figure 7b). Only one exception was found: Mtm05Na_3W exhibited higher frequency of the sharp peak than Mtm03Na_3W. In contrary to the experimental observations (Kuligiewicz *et al.*, 2015a), the position of the high-frequency peak was found to depend on charge location and water content.

=== Figure 7 ===

In addition, the MD results showed a substantial difference in peak position between the Na^+ and Ca^{2+} forms of smectites (Figure 7b), which are not visible experimentally (Figure 7c, Kuligiewicz *et al.*, 2015a). Also the peak positions of the Cs^+ forms exhibited trends in relation to Na^+ and Ca^{2+} forms that are different in MD than in experiment.

These discrepancies between the experimental trends and the outcome of MD simulations can be related to the approximations involved in the latter, primarily in certain features of the CLAYFF model (Cygan *et al.*, 2004). The Lennard-Jones parameters of Ferrage *et al.* (2011) should be more accurately optimized, the hexagonal cavity in the tetrahedral sheet ought to have lower ditrigonal symmetry. A better description of the structure would affect the distribution and orientation of H_2O. The model for H_2O may also have limitations and the power spectra have excessive high-frequency spectral density at 3728 cm^{-1}. Finally, uncertainties introduced by the fitting procedure can be observed (Figure 6). In spite of all these limitations, the overall picture is relatively consistent: All the studied smectites exhibit a stretching band at lower frequencies and this band shift to lower energy upon increasing layer charge (Figure 7ab).

Molecular origin of the sharp O-D_w/O-H_w band

Calculations of the power spectra of specific sub-sets of interlayer water hydrogen atoms were performed in order to explain in more detail which part of the surface H_2O population is responsible for the sharp high-frequency vibrational band observed in the experimental spectra (Kuligiewicz *et al.*, 2015a). Each subset was defined by a common range of distances from the surface, z, and H_2O dipole orientation angle, α (Figure 1). A H_2O molecule belongs to a certain sub-set if it is found within the same (z, α) range in both the first and the last time-window of the VACF calculation. The results for three representative smectites (Mtm03Na_2W, Beid03Na_2W and Mtm05Ca_2W) are presented in Figure 8. Spectral intensities were scaled by the number of H_2O molecules identified in each subset in order to compare the contribution of each subset to the total spectrum.

=== Figure 8 ===

This analysis demonstrates that H_2O molecules at the center of the interlayer are not responsible for producing the sharp spectral feature. The latter originates instead from the overlapping contributions of both monodentate and bidentate orientations of surface H_2O. The contribution of the monodentate orientation is, however, much stronger because of the higher number of H_2O molecules populating this sub-set. If present, bidentate H_2O gives a very small, although non-negligible, contribution to the power spectrum at frequencies that are on average higher than those of the monodentate population.

Based on the correlation of IR frequency of the O-H stretching band and the length of the H-bond, $O\text{-}H_w\cdots O$, (Libovitzky, 1999), a peak at ~ 3600 cm^{-1} may correspond to a $O\text{-}H_w\cdots O$ distance > 2.2 Å (i.e. an $O_w ... O$ distance >3.2 Å), and indicates a relatively weak H-bond donated to the surface (e.g., Kalinichev, 2001; Kumar *et al.*, 2007). Therefore, in order to obtain deeper insight into the studied problem, the distribution of the shortest $O_w\text{-}H_w\cdots O_b$ distances in the monodentate and bidentate sub-sets were calculated (Figure 8, right column). The results showed a relatively broad distribution of the distances, with the maximum for monodentate H_2O at ~1.9 Å for Beid03_Na and Mtm05Ca_2W, and ~2.0 Å for Mtm03Na_2W. For comparison, in bulk liquid water the maximum of the shortest $O_w\text{-}H_w\cdots O_w$ distance is at ~1.8 Å (e.g., Kalinichev, 2001; Kumar *et al.*, 2007). The weighted average of the calculated $O_w\text{-}H_w\cdots O_b$ distributions is, however, a little bit greater than the maxima: 2.24 Å for Beid03_Na, 2.16 Å for Mtm05Ca_2W, and 2.27 Å for Mtm03Na_2W, comparing to 1.95 Å in bulk water. In bulk water a contribution of H-bond distances > 2.2 Å was observed, but this is much smaller than for smectites. Low charge smectites exhibited a significantly larger contribution of weak H-bonds. For the high charge smectite Mtm05Ca_2W the contribution of weak H-bonds due to H_2O molecules in monodentate orientation was noticeably smaller. This explains the higher frequency and intensity of the high-frequency monodentate peak in the vibrational spectrum of this smectite. In the case of bidentate population, one of the $O\text{-}H_w\cdots O_b$ distances had a maximum also at ~1.9-2.0 Å, resulting in an H-bond of a comparable strength, while the second one was significantly longer and, respectively, weaker. This analysis suggests that upon increasing total layer charge the H-bond distances of the bidentate sub-set are decreasing and causing the red-shift of the calculated power spectrum.

Due to its ubiquitous presence and relative abundance, the population of monodentate surface H_2O is mainly responsible for the presence of the sharp high-frequency OH stretching feature observed in the experiments (Kuligiewicz *et al.*, 2015a). This is in very good agreement with earlier experimental data (e.g., Russell and Farmer 1964; Farmer and Russell 1971; Prost 1975; Suquet *et al.*, 1977; Sposito and Prost 1982; Sposito *et al.*, 1983) which linked the high frequency band to H_2O at the surface of the interlayer, pointing one of their $O\text{-}H_w$ bonds towards the siloxane surface. In certain cases the bidentate sub-population may provide a non-negligible contribution as observed for higher charged smectites, e.g., for Mtm05_Ca_2W.

Possible alternative molecular mechanisms responsible for the sharp O-Dw/O-Hw band

Evidence from MD simulations in support of the experimental data, suggested that the sharp high-frequency band in the IR spectra of hydrated smectite is clearly originating from H_2O molecules oriented towards the clay surface. Can there be any other contribution to this sharp IR band? One possibility that would also be linked to surface H_2O, could, for example, involve the second O-H_w bond of monodentate H_2O, i.e. the one oriented towards the middle of the interlayer, away from the siloxane surface. As the surface H_2O molecules have relatively fixed orientations, their O-H_w bonds that are pointing away from the surface might have a decreased number of available H-bond acceptors within a suitable range and orientation around them. Such a lower coordination could, in principle, contribute in part to the observed sharp high-frequency infrared band. To examine this possibility, the subsets representing two separate hydroxyls of the monodentate population in Mtm05Ca_2W and Mtm05Na_2W were investigated (Figure 9).

=== Figure 9 ===

In the case of monodentate H_2O, one H-bond is donated to the surface (thick blue rectangle in Figure 9), while the second one is donated to another H_2O (dashed orange rectangle in Figure 9). The corresponding power spectra show that only the hydrogens oriented towards the surface contribute to the high-frequency band. The power spectrum of the second hydrogen resembles that of bulk water, with even a slightly higher intensity of the vibrational band at lower frequency ~3500 cm^{-1}, indicating a relatively strong H-bonding to other interlayer H_2O molecules. This is additionally confirmed by comparison of the shortest O_w-$H_w\cdots O_w$ distances of this sub-population and the corresponding distances in pure water (right column in Figure 9). The two distributions are practically identical.

A second mechanism potentially responsible for the emergence of the high-frequency H_2O stretching band could be related to the influence of interlayer cations. The latter could deform the H-bonding structure of H_2O molecules around them and possibly induce some H-bond breaking. A clear evidence against this possibility has been provided already in Figure 8: H_2O molecules in the middle of the interlayer (red rectangle) were found not to contribute to the high-frequency band of interest. This is especially obvious in the case of Mtm05Ca_2W, where H_2O molecules in the hydration shell of Ca^{2+} are oriented around the ions exactly in the center of the interlayer.

Hydrogen bonding in the interlayer space of smectite

The question regarding other possible molecular mechanisms responsible for the sharp high-frequency O-D_w/O-H_w band can be alternatively expressed as follows: Does interlayer water contain a sub-population of H_2O molecules for which the O-$H_w\cdots$O distance of donated H-bonds is longer than ~2.2 Å (Libovitzky, 1999)? Obviously, the results of this analysis are only valid in comparison to those on pure bulk liquid water, due to the method-artificial non-negligible contribution of weak H-bonds in the latter (see Figure 8 and 9).

To address this question, the numbers of accepted and donated H-bonds were calculated depending on the distance *z* of the involved H_2O molecules from the smectite siloxane surface. In the ordered ice structure, each H_2O donates two strong H-bonds to other H_2O and also accepts two strong H-bonds from two other H_2O molecules. In liquid water, the number of donating and accepting H-bonds formed by each H_2O molecule is somewhat lower than in ice due to the molecular disorder, and depends on temperature, density, and other thermodynamic factors. The exact number of H-bonds experienced by a H_2O molecule in each situation also depends to some extent on the assumed criterion used in H-bonding calculation (see., e.g., Kalinichev, 2001; Kumar *et al.*, 2007).

A geometric definition for counting H-bonds (HB) was adopted from the literature (Wang *et al.,* 2009; Loganathan and Kalinichev, 2013). According to this definition, an H-bond is assumed to exist if the H$\cdots$O distance between the donor and acceptor is below 2.45 Å and the angle between the O–H and O$\cdots$O vectors is below 30°. A systematic application of this criterion enabled the quantitative visualization of the general H-bonding trends of interlayer H_2O molecules for several model smectites (Figure 10). As expected, H-bonds donated to surface O_b atoms from both bidentate and monodentate H_2O populations were identified in all cases (thick solid lines in Figure 10). The maximum of their distribution corresponded to the monodentate population, whereas the small shoulder closer to the surface originated from bidentate H_2O. Besides donating to the basal surface, both bidentate and monodentate H_2O accepted H-bonds from and donated to other H_2O in the interlayer (dashed and thin solid lines, respectively in Figure 10). The maxima of the accepted and donated H-bonding distributions corresponded clearly to the expected (e.g., Ferrage *et al.*, 2011; Ngouana Wakou and Kalinichev, 2014) twin maxima of the O_w distribution along *z,* shown previously for all 2W structures (Figures 2 and 3). Subtler differences in the fractions of accepting and donating H-bonds depended on the charge and the type of the interlayer cation (Figure 10).

=== Figure 10 ===

The distributions of H-bonds along *z* (Figure 10) provide a general picture of the H-bonding structure in smectite interlayers, but they do not directly indicate the location of particularly weak hydrogen bonds. To address this issue, the distributions of H-bonds on the basis of their strength was also calculated (Figure 11). This was achieved by modifying the aforementioned geometric definition of H-bond to probe only the relatively weak interactions having O_w-H···O distances in the range 2.2-2.7 Å and compare such a subset of the H-bonds distribution to the original definition (O_w-H···O distance <2.45 Å). In both cases the H-O_w···O angle was kept $< 30^o$. The plots in Figure 11 show only the average distributions of H-bonds experienced by each H_2O molecule, and therefore do not inform on the absolute contribution of each molecular orientation to the final spectra.

=== Figure 11 ===

For the general case considering all possible H-bonds in the system (Figure 11a), the number of accepted H-bonds per H_2O molecule was found relatively constant with small dependence on the smectite charge and the type of the interlayer cation (dashed lines in Figure

11a). The number of H-bonds donated to basal oxygen atoms was around 2.0 per H_2O molecule for the bidentate orientation and slightly below 1.0 for the monodentate orientation for all types of simulated smectite systems (thick solid lines in Figure 11a). The number of H-bonds per H_2O donated to other H_2O was independent of charge and interlayer cation (thin solid line in Figure 11a).

The average number of weak H-bonds calculated according to the modified geometric criterion also did not show substantial dependence on the type of smectite (Figure 11). The weakest H-bonds (0.8-1.0 of donated H-bonds per H_2O; thick solid line in Figure 11b) was clearly attributed to the bidentate orientation, but some contribution from the monodentate population, amounting to ~0.3 donated H-bonds per H_2O was also observed. For comparison, the average number of weak H-bonds in bulk liquid water, calculated using the same criteria was ~0.17 per molecule. Therefore, only the fraction of weak H-bonds that is in excess of the value of ~0.17 per molecule can be considered as contributing to the sharp high-frequency vibrational band. In agreement with the calculated power spectra, these H-bonds are solely due to the bidentate and monodentate populations in the vicinity of the surface and no contribution from the central part of the interlayer was found.

CONCLUSIONS

(1) Interfacial water molecules in bidentate and monodentate orientation with respect to the siloxane surface are the only species contributing to the experimentally observed sharp high-frequency O-H_w stretching band of smectites (Kuligiewicz *et al.*, 2015a, Kuligiewicz *et al.*, 2015b). The number of interlayer H_2O molecules in the monodentate orientation greatly exceeds that in the bidentate orientation and is, thus, the predominant contributor to the high-frequency vibrational band.

(2) In the bidentate orientation each H_2O molecule donates two hydrogen bonds to the surface: one relatively strong, and another much weaker, while in the monodentate orientation it donates only one relatively weak H-bond to the surface.

(3) Increasing total layer charge leads to increasing number of bidentate molecules, but also to decreasing of O_w-H···O_b distances for both monodentate and bidentate populations. Both factors are responsible for the red-shift of the sharp high-frequency band in smectites upon increasing the layer charge.

(4) The experimentally observed low sensitivity of the position of the high-frequency vibrational band on the type of the (Na^+ or Ca^{2+}) high hydration enthalpy interlayer cation remains unexplained. The differentiation of Cs^+ from Na^+ or Ca^{2+} may be due to its tendency to displace surface H_2O and form inner-sphere complexes with the siloxane surface as suggested by Kuligiewicz *et al.* (2015a), but further simulation work is needed to account for the experimental data on Cs^+ smectites.

(5) The presence of the sharp high-frequency vibrational band in experimental and simulated spectra can be considered as a strong evidence of intrinsic hydrophobicity of the smectite siloxane surface within the studied range of layer charge (0.3-0.5 phuc), independent on the specific charge localization in the clay structure.

ACKNOWLEDGMENTS

This work was supported by the project ATLAB (FP7-REGPOT-2011-1 No. 285989) funded by the European Union. MS also acknowledges NCN (grant 2012/05/B/ST10/01948), which provided IGS PAS with a high-performance computing server and also PLGRID infrastructure. AGK acknowledges the support of the industrial chair “Storage and Disposal of Radioactive Waste” at the Ecole des Mines de Nantes, funded by ANDRA, Areva, and

EDF. VG and GDC acknowledge partial support from project KRHPIS 447963 -Polynano (GSRT, TPCI-NHRF).

REFERENCES

Allen, M.P. and Tildesley, D.J. (1987) *Computer Simulation of Liquids*. Oxford University Press, New York, 385pp.

Arab, M., Bougeard, D., and Smirnov, K.S. (2003) Structure and dynamics of the interlayer water in an uncharged 2 : 1 clay. *Physical Chemistry Chemical Physics*, **5**, 4699-4707.

Boek, E.S., Coveney, P.V., and Skipper, N.T. (1995) Monte Carlo molecular modeling studies of hydrated Li-, Na-, and K-smectites: Understanding the role of potassium as a clay swelling inhibitor. *Journal of the American Chemical Society,* **117**, 12608-12617.

Boek, E.S. and Sprik, M. (2003) Ab initio molecular dynamics study of the hydration of a sodium smectite clay. *Journal of Physical Chemistry B,* **107**, 3251-3256.

Bridgeman, C.H. and Skipper, N.T. (1997) A Monte Carlo study of water at an uncharged clay surface. *Journal of Physics-Condensed Matter*, **9**, 4081-4087.

Cariati, F., Erre, L., Micera, G., Piu, P., and Gessa, C. (1981) Water molecules and hydroxyl groups in montmorillonites as studied by near infrared spectroscopy. *Clays and Clay Minerals*, **29**, 157-159.

Cariati, F., Erre, L., Micera, G., Piu, P., and Gessa, C. (1983) Polarization of water molecules in phyllosilicates in relation to exchange cations as studied by near infrared spectroscopy. *Clays and Clay Minerals*, **31**, 155-157.

Cases, J.M., Berend, I., Francois, M., Uriot, J.P., Michot, L.J., and Thomas, F. (1997) Mechanism of adsorption and desorption of water vapor by homoionic montmorillonite. 3. The Mg^{2+}, Ca^{2+}, Sr^{2+} and Ba^{2+} exchanged forms. *Clays and Clay Minerals*, **45**, 8-22.

Chang, F.R.C., Skipper, N.T., and Sposito, G. (1995) Computer simulation of interlayer molecular structure in sodium montmorillonite hydrates. *Langmuir*, **11**, 2734-2741.

Churakov, S.V. (2006) Ab initio study of sorption on pyrophyllite: Structure and acidity of the edge sites. *Journal of Physical Chemistry B*, **110**, 4135-4146.

Cygan, R.T., Liang, J.J., and Kalinichev, A.G. (2004) Molecular models of hydroxide, oxyhydroxide, and clay phases and the development of a general force field. *Journal of Physical Chemistry B*, **108**, 1255-1266.

Dazas, B., Ferrage, E., Delville, A., and Lanson, B. (2014) Interlayer structure model of tri-hydrated low-charge smectite by X-ray diffraction and Monte Carlo modeling in the Grand Canonical ensemble. *American Mineralogist*, **99**, 1724-1735.

Dazas, B., Lanson, B., Delville, A., Robert, J.L., Komarneni, S., Michot, L.J., and Ferrage, E. (2015) Influence of tetrahedral layer charge on the organization of interlayer water and ions in synthetic Na-saturated smectites. *Journal of Physical Chemistry C*, **119**, 4158-4172.

Efimov, Y.Y. and Naberhukhin, Y.I. (2002) On the interrelation between frequencies of stretching and bending vibrations in liquid water. Spectrochimica Acta A, **58**, 519 - 524.

Farmer, V.C. and Russell, J.D. (1971) Interlayer complexes in layer silicates: The structure of water in lamellar ionic solutions. *Transactions of the Faraday Society*, **67**, 2737-2749.

Ferrage, E., Lanson, B., Sakharov, B.A., and Drits, V.A. (2005) Investigation of smectite hydration properties by modeling experimental X-ray diffraction patterns: Part I. Montmorillonite hydration properties. *American Mineralogist*, **90**, 1358-1374.

Ferrage, E., Lanson, B., Sakharov, B.A., Geoffroy, N., Jacquot, E., and Drits, V.A. (2007) Investigation of dioctahedral smectite hydration properties by modeling of X-ray diffraction profiles: Influence of layer charge and charge location. *American Mineralogist*, **92**, 1731-1743.

Ferrage, E., Sakharov, B.A., Michot, L.J., Delville, A., Bauer, A., Lanson, B., Grangeon, S., Frapper, G., Jiménez-Ruiz, M., and Cuello, G.J. (2011) Hydration properties and interlayer organization of water and ions in synthetic Na-smectite with tetrahedral layer charge. Part 2. Toward a precise coupling between molecular simulations and diffraction data. *Journal of Physical Chemistry C*, **115**, 1867-1881.

Greathouse, J.A. and Sposito, G. (1998) Monte Carlo and molecular dynamics studies of interlayer structure in $Li(H_2O)_3$–smectites. *Journal of Physical Chemistry B*, **102**, 2406-2414.

Greathouse, J.A., Durkin, J.S., Larentzos, J.P., and Cygan, R.T. (2009) Implementation of a Morse potential to model hydroxyl behavior in phyllosilicates. *Journal of Chemical Physics*, **130**, 134713.

Greathouse, J.A., Hart, D.B., Bowers, G.M., Kirkpatrick, R.J., and Cygan, R.T. (2015) Molecular simulation of structure and diffusion at smectite-water interfaces: Using expanded clay interlayers as model nanopores. *Journal of Physical Chemistry C*, **119**, 17126-17136.

Guillot, B. (2002) A reappraisal of what we have learnt during three decades of computer simulations on water. *Journal of Molecular Liquids*, **101**, 219-260.

Jaynes, W.F. and Boyd, S.A. (1991) Hydrophobicity of siloxane surfaces in smectites as revealed by aromatic hydrocarbon adsorption from water. *Clays and Clay Minerals*, **39**, 428-436.

Kalinichev, A.G. (2001) Molecular simulations of liquid and supercritical water: Thermodynamics, structure, and hydrogen bonding. *Reviews in Mineralogy and Geochemistry*, **42**, 83-129.

Kleinhesselink, D. and Wolfsberg, M. (1992) The evaluation of power spectra in molecular dynamics simulations of anharmonic solids and surfaces. *Surface Science*, **262**, 189-207.

Kuligiewicz, A., Derkowski, A., Szczerba, M., Gionis, V., and Chryssikos, G.D. (2015a)

Water-smectite interface by infrared spectroscopy, *Clays and Clay Minerals*, **63**, 15-29.

Kuligiewicz, A., Derkowski, A., Emmerich, K., Christidis, G. E., Tsiantos, C., Gionis, V., and Chryssikos, G. D. (2015b) Measuring the Layer Charge of Dioctahedral Smectite by O–D Vibrational Spectroscopy. *Clays and Clay Minerals*, **63**, 443-456.

Kumar, R., Schmidt, J.R., and Skinner, J.L. (2007) Hydrogen bonding definitions and dynamics in liquid water. *Journal of Chemical Physics*, **126**, 204107-12.

Lee, J.H. and Guggenheim, S., (1981) Single crystal X-ray refinement of pyrophyllite-1Tc. *American Mineralogist*, **66**, 350–357.

Libowitzky, E. (1999) Correlation of O-H stretching frequencies and O-H···O bond lengths in minerals. *Monatshefte für Chemie*, **130**, 1047-1059.

Loganathan, N. and Kalinichev, A.G. (2013) On the hydrogen bonding structure at the aqueous interface of ammonium-substituted mica: A molecular dynamics simulation. *Zeitschrift für Naturforschung A*, **68**, 91-100.

Loganathan, N., Yazaydin, A.O., Bowers, G.M., Kalinichev, A.G., and Kirkpatrick, R.J. (2016a) Structure, energetics, and dynamics of Cs^+ and H_2O in hectorite: Molecular dynamics simulations with an unconstrained substrate surface. *Journal of Physical Chemistry C*, **120**, 10298-10310.

Loganathan, N., Yazaydin, A.O., Bowers, G.M., Kalinichev, A.G., and Kirkpatrick, R.J. (2016b) Cation and water structure, dynamics, and energetics in smectite clays: A molecular dynamics study of Ca-hectorite. *Journal of Physical Chemistry C*, **120**, 12429-12439.Löwenstein, W. (1954) The distribution of aluminum in the tetrahedral of silicates and aluminates, *American Mineralogist*, **39**, 92-96.

Madejová, J., Janek, M., Komadel, P., Herbert, H.-J., and Moog, H.C. (2002) FTIR analyses of water in MX-80 bentonite compacted from high salinary salt solution systems.

Applied Clay Science, **20**, 255-271.

Marry, V., Rotenberg, B., and Turq, P. (2008) Structure and dynamics of water at a clay surface from molecular dynamics simulation. *Physical Chemistry Chemical Physics*, **10**, 4802-4813.

Marry, V., Dubois, E., Malikova, N., Breu, J., and Haussler, W. (2013) Anisotropy of water dynamics in clays: Insights from molecular simulations for experimental QENS analysis. *Journal of Physical Chemistry C*, **117**, 15106–15115.

Michot, L.J., Villieras, F., Francois, M., Yvon, J., Le Dred, R., and Cases, J.M. (1994) The structural microscopic hydrophilicity of talc. *Langmuir*, **10**, 3765-3773.

Morrow, C.P., Yazaydin, A.O., Krishnan, M., Bowers, G.M., Kalinichev, A.G., and Kirkpatrick, R.J. (2013) Structure, energetics, and dynamics of smectite clay interlayer hydration: molecular dynamics and metadynamics investigation of Na-hectorite. *Journal of Physical Chemistry C*, **117**, 5172-5187.

Ngouana Wakou, B.F. and Kalinichev, A.G. (2014) Structural arrangements of isomorphic substitutions in smectites: Molecular simulation of the swelling properties, interlayer structure, and dynamics of hydrated Cs–montmorillonite revisited with new clay models. *Journal of Physical Chemistry C*, **118**, 12758-12773

Ortega-Castro, J., Hernández-Haro, N., Dove, M.T., Hernández-Laguna, A., and Saínz-Diaz, C.I. (2010) Density functional theory and Monte Carlo study of octahedral cation ordering of Al/Fe/Mg cations in dioctahedral 2:1 phyllosilicates. *American Mineralogist*, **95**, 209–220.

Plimpton, S. (1995) Fast parallel algorithms for short-range molecular dynamics. *Journal of Computational Physics*, **117**, 1–19.

Praprotnik, M., Janezic, D., and Mavri, J. (2004) Temperature dependence of water vibrational spectrum: A molecular dynamics simulation study. *Journal of Physical*

Chemistry A, **108**, 11056–11062.

Prost, R. (1975) Interactions between adsorbed water molecules and the structure of clay minerals: Hydration mechanism of smectites. *Proceedings of International Clay Conference of The Clay Minerals Society, Mexico City*, 351-359.

Rotenberg, B., Patel, A.J., and Chandler, D. (2011) Molecular explanation for why talc surfaces can be both hydrophilic and hydrophobic. *Journal of the American Chemical Society*, **133**, 20521-20527.

Russell, J.D. and Farmer, V.C. (1964) Infrared spectroscopic study of the dehydration of montmorillonite and saponite. *Clay Minerals Bulletin*, **5**, 443-464.

Sato, T., Watanabe, T., and Otsuka, R. (1992) Effects of layer charge, charge location, and energy change on expansion properties of dioctahedral smectites. *Clays and Clay Minerals*, **40**, 103-113.

Skipper, N.T., Soper, A.K., and McConnell, J.D.C. (1991) The structure of interlayer water in vermiculite. *Journal of Chemical Physics*, **94**, 5751-5760.

Sobolev, O., Favre Buivin, F., Kemner, E., Russina, M., Beuneu, B., Cuello, G.J., and Charlet, L. (2010) Water-clay surface interaction: A neutron scattering study. *Chemical Physics*, **374**, 55-61.

Šolc, R., Gerzabek, M.H., Lischka, H., and Tunega, D. (2011) Wettability of kaolinite (001) surfaces - Molecular dynamic study. *Geoderma*, **169**, 47-54.

Sovago, M., Kramer Campen, R.K., Bakker H.J., and Bonn, M. (2009) Hydrogen bonding strength of interfacial water determined with surface sum-frequency generation. *Chemical Physics Letters*, **470**, 7 - 12.

Sposito, G. and Prost, R. (1982) Structure of water adsorbed on smectites. *Chemical Reviews*, **82**, 554-573.

Sposito, G., Prost, R., and Gaultier, J.-P. (1983) Infrared spectroscopic study of adsorbed water on reduced-charge Na/Li-montmorillonites. *Clays and Clay Minerals*, **31**, 9-16.

Sposito, G., Skipper, N.T., Sutton, R., Park, S-H., Soper, A.K., and Greathouse, J.A. (1999) Surface geochemistry of clay minerals. *Proceedings of National Academy of Science USA*, **96**, 3358-3364.

Suquet, H., Prost, R., and Pezerat, H. (1977). Etude par la spectroscopie infrarouge de l' eau adsorbée par la saponite-calcium. *Clay Minerals*, **12**, 113-125.

Suzuki, S. and Kawamura, K. (2004) Study of vibrational spectra of interlayer water in sodium beidellite by molecular dynamics simulations. *Journal of Physical Chemistry B*, **108**, 13468-13474.

Środoń, J. and McCarty, D.K. (2008) Surface area and layer charge of smectite from CEC and EGME/H_2O retention measurements. *Clays and Clay Minerals,* **56**, 155-174.

Szczerba, M., Kłapyta, Z., and Kalinichev, A.G. (2014) Ethylene glycol intercalation in smectites. Molecular dynamics simulation studies. *Applied Clay Science*, **91**, 87-97.

Tay, K. and Bresme, F. (2006) Hydrogen bond structure and vibrational spectrum of water at a passivated metal nanoparticle. *Journal of Materials Chemistry*, **16**, 1956–1962.

Teich-McGoldrick, S.L., Greathouse, J.A., Jové-Colón, C.F., and Cygan, R.T. (2015) Swelling properties of montmorillonite and beidellite clay minerals from molecular simulation: Comparison of temperature, interlayer cation, and charge location effects. *Journal of Physical Chemistry C*, **119**, 20880-20891.

Toukan, K. and Rahman, A. (1985) Molecular-dynamics study of atomic motions in water. *Physical Review B,* **31**, 2643–2648.

Tunega, D., Gerzabek, M.H. and Lischka, H. (2004) Ab initio molecular dynamics study of a monomolecular water layer on octahedral and tetrahedral kaolinite surfaces. *Journal of Physical Chemistry B*, **108**, 5930-5936.

Wang, J.W., Kalinichev, A.G., and Kirkpatrick, R.J. (2004) Molecular modeling of the 10-angstrom phase at subduction zone conditions. *Earth and Planetary Science Letters*, **222**, 517-527.

Wang, J.W., Kalinichev, A.G., and Kirkpatrick, R.J. (2005a) Structure and decompression melting of a novel, high-pressure nanoconfined 2-D ice. *Journal of Physical Chemistry B*, **109**, 14308-14313.

Wang, J., Kalinichev, A.G., Kirkpatrick, R.J., and Cygan, R.T. (2005b) Structure, energetics, and dynamics of water adsorbed on the muscovite (001) surface: a molecular dynamics simulation. *The Journal of Physical Chemistry B*, **109**, 15893-15905.

Wang, J., Kalinichev, A.G., and Kirkpatrick, R.J. (2009) Asymmetric hydrogen bonding and orientational ordering of water at hydrophobic and hydrophilic surfaces: A comparison of water/vapor, water/talc, and water/mica interfaces. *Journal of Physical Chemistry C,* **113**, 11077-11085.

Xu, W., Johnston, C.T., Parker, P., and Agnew, S.F. (2000) Infrared study of water sorption on Na-, Li-, Ca- and Mg-exchanged (SWy-1 and SAz-1) montmorillonite. *Clays and Clay Minerals*, **48**, 120-131.

Zaunbrecher, L.K., Cygan, R.T., and Elliott, W.C. (2015) Molecular models of cesium and rubidium adsorption on weathered micaceous minerals. *Journal of Physical Chemistry A*, **119**, 5691-5700.

Table 1. Parameters of interatomic interactions used in present MD simulations. The modifications compared to the original CLAYFF parameters (Table 1 in Cygan *et al.*, 2004) are highlighted in bold.

Species	charge (*e*)	D_0 (kcal/mol)	R_0 (Å)
surface bridging O	-1.05000	0.1554	**3.8000**
surface bridging O near tetrahedral substitution	-1.16875	0.1554	**3.8000**
ordinary bridging O	-1.05000	0.1554	3.5532
ordinary bridging O near tetrahedral substitution	-1.16875	0.1554	3.5532
ordinary bridging O near octahedral substitution	-1.18085	0.1554	3.5532
tetrahedral aluminum	1.57500	$1.8405\cdot10^{-6}$	**3.4596**
tetrahedral silicon	2.10000	$1.8405\cdot10^{-6}$	**3.4596**
octahedral aluminum	1.05000	$1.3298\cdot10^{-6}$	4.7943
octahedral magnesium	1.05000	$9.0298\cdot10^{-7}$	5.9090
hydroxyl oxygen	-0.95000	0.1554	3.5532
hydroxyl hydrogen	0.42500	0.0	0.0
aqueous sodium ion	1.00000	0.1301	2.6378
aqueous calcium ion	2.00000	0.1000	3.2237
aqueous cesium ion	1.00000	0.1000	4.3002

Table 2. Interlayer cation and water content of the simulated clay models and the resulting basal spacing.

Model	$n(H_2O)$ phuc	$n(H_2O)/n(M^+)$	H_2O wt% normalized to the total mass (smectite + H_2O)	H_2O wt% normalized to dry mass (smectite)	calculated d_{001} (Å)*
Beid03Na_1W	2.5	8.333	10.93	12.28	12.99
Beid03Na_2W	5	16.667	19.71	24.55	15.94
Beid03Na_3W	7.5	25.0	26.92	36.83	18.88
Beid05Na_1W	2.5	5.0	10.82	12.13	12.76
Beid05Na_2W	5.0	10.0	19.53	24.26	15.38
Beid05Na_3W	7.5	15.0	26.68	36.39	18.34
Mtm03Na_1W	2.5	8.333	10.95	12.29	12.86
Mtm03Na_2W	5.0	16.667	19.73	24.58	15.95
Mtm03Na_3W	7.5	25.0	26.94	36.88	18.95
Mtm05Na_1W	2.5	5.0	10.84	12.16	12.58
Mtm05Na_2W	5.0	10.0	19.56	24.31	15.37
Mtm05Na_3W	7.5	15.0	26.72	36.47	18.14
Beid03Ca_2W	5.0	33.334	19.75	24.61	15.82
Beid05Ca_2W	5.0	20.0	19.59	24.36	15.38
Mtm03Ca_2W	5.0	33.334	19.77	24.64	15.95
Mtm05Ca_2W	5.0	20.0	19.62	24.41	15.38
Beid03Cs_2W	5.0	16.667	18.39	22.53	16.34
Beid05Cs_2W	5.0	10.0	17.45	21.13	16.13
Mtm03Cs_2W	5.0	16.667	18.40	22.55	16.41
Mtm05Cs_2W	5.0	10.0	17.47	21.17	16.14

$^{*)}$Standard deviation is ~ ± 0.05 Å.

FIGURE CAPTIONS

Figure 1. A snapshot of part of the MD simulation cell for Mtm05Na_3W. H_2O closer to the layer surface is oriented with two O-H_w bonds pointing to the surface (thin green circle), whereas H_2O farther from the surface - with one O-H_w bond oriented towards the surface (thick blue circle). The inset shows the definition of the angle α formed by the H_2O dipole vector and the surface normal. Vertical scale showing average distance in z direction relative to the oxygens of the basal plane is shown in angstroms.

Figure 2. Dependence of the H_2O dipole vector orientation contours (see Figure 1 for the definition of α) on the distance from the basal surface, z, for various hydration levels of different Na^+-smectites. The interlayer distribution of the cations is shown by solid lines (blue in the color copy). Dashed lines mark the location of the surface (basal oxygen positions).

Figure 3. Dependence of the H_2O dipole orientation contours on the distance from the basal surface, z, for 2W hydration level of Ca^{2+} and Cs^+-smectites.

Figure 4. Power spectra for hydrogens of interlayer H_2O in smectites with two hydration layers (2W) in the O-H_w stretching range showing the effect of the total layer charge and the cation-dependence: a) Na^+ form, b) Ca^{2+} form, c) Cs^+ form. Increase of the spectral density at higher frequency is clearly visible in comparison with the spectrum of bulk water.

Figure 5. Power spectra for hydrogens of interlayer H_2O in the O-H_w stretching range for Na^+-beidellites (top) and Na^+-montmorillonites (bottom) with different total layer charge and different water contents. The spectra were scaled by their H_2O content.

Figure 6. ~~Examples of received fits~~Deconvolution of power spectra ~~for~~ of pure water and two representative smectites.

Figure 7. Comparison of ~~fitted~~ frequencies: a) dependence on water content for Na^+-smectites in MD; b) dependence on interlayer cation for 2W forms in MD~~.~~; ~~c)~~ in comparison to c) results from Kuligiewicz et al. (2015a). To obtain frequencies for H_2O, the experimental values for D_2O were scaled by ~~factor of~~x 1.36.

Figure 8. H_2O dipole orientation with respect to the surface normal for selected sub-sets of water molecules having their z and α values within the marked ranges (left) and power spectra of O-H_w stretching vibrations calculated for each individual sub-set (center): thin green – bidentate population, thick blue – monodentate population, dashed red – water in the center of interlayer. Right column – the distributions of the shortest H-bonding distances of interfacial H_2O molecules with basal oxygens (O_w-$H_w\cdots O_b$) in the bidentate and monodentate orientations, compared to distribution of O_w-$H_w\cdots O_w$ distances in pure water.

Figure 9. Orientation of the O-H_w vector of interfacial H_2O with respect to the surface normal (β) at various distances, z, from the basal surface of Mtm05Ca_2W and Mtm05Na_2W smectites (left). Calculated power spectra for the sub-sets of H_2O molecules (color marked for the selected β and z ranges) are shown in the center. Right: the distributions of the shortest H-bonding distances of monodentate H_2O with the basal oxygens (O_w-$H_w\cdots O_b$) and/or other oxygen of H_2O (O_w-$H_w\cdots O_w$), compared to distribution of O_w-$H_w\cdots O_w$ distances in pure water. Thin green – bidentate population, thick blue – water O-H_w bond oriented towards the surface, dashed orange – O-H_w bond oriented towards the interlayer. Power spectra were scaled by the number of H_2O molecules. A bulk water spectrum is also shown for comparison.

Figure 10. Distributions of O_w atoms with H-bonds ~~donated and~~ accepted and donated by the interlayer H_2O and O_b in the 2W smectite structures studied.

Figure 11. Distributions of O_w atoms with H-bonds of various types (normalized per one H_2O) for the 2W smectite structures studied. (a) - all H-bonds with O_w-$H\cdots O$ distances below 2.45 Å. (b) - weak (long) H-bonds with O_w-$H\cdots O$ distances in the range of 2.2-2.7 Å. In both cases the H-$O_w\cdots O$ angle is < 30^o.

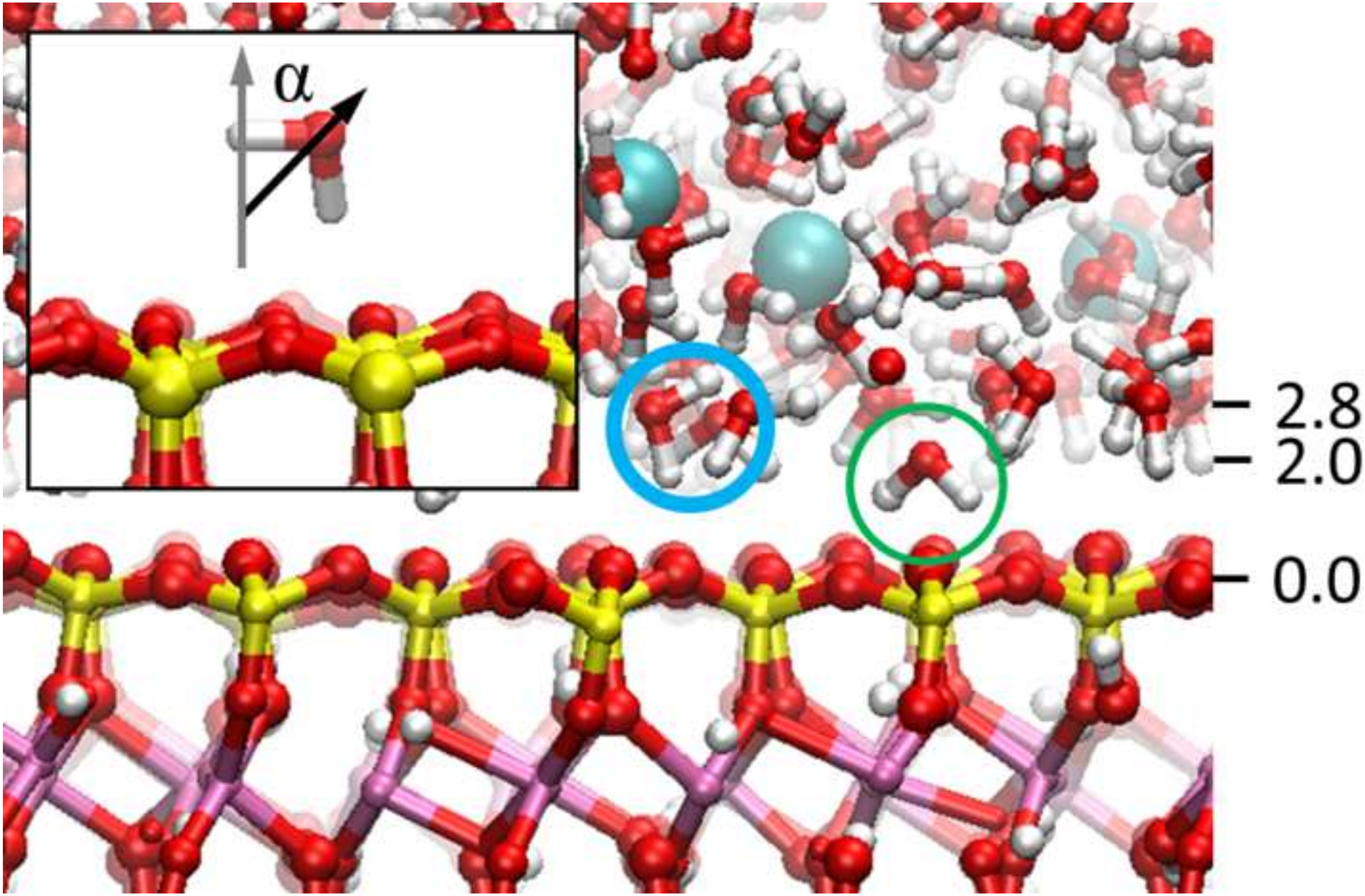
α
2.8
2.0
0.0

Figure_2

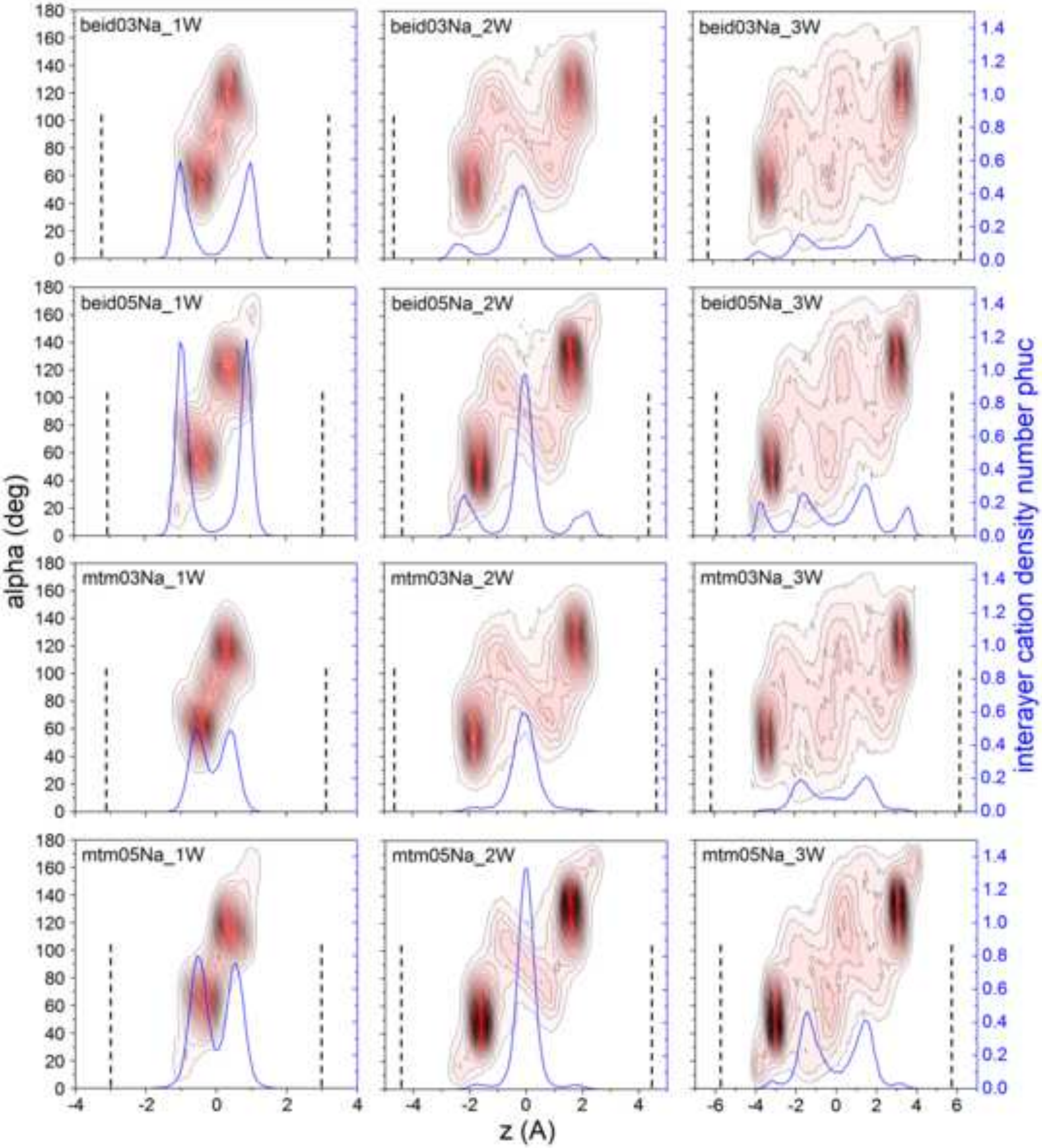
beid03Na_1W
beid03Na_2W
beid03Na_3W
beid05Na_1W
beid05Na_2W
beid05Na_3W
mtm03Na_1W
mtm03Na_2W
mtm03Na_3W
mtm05Na_1W
mtm05Na_2W
mtm05Na_3W
alpha (deg)
interayer cation density number phuc
z (A)
0
20
40
60
80
100
120
140
160
180
0.0
0.2
0.4
0.6
0.8
1.0
1.2
1.4
-4
-2
0
2
4
-6
6

Figure_3

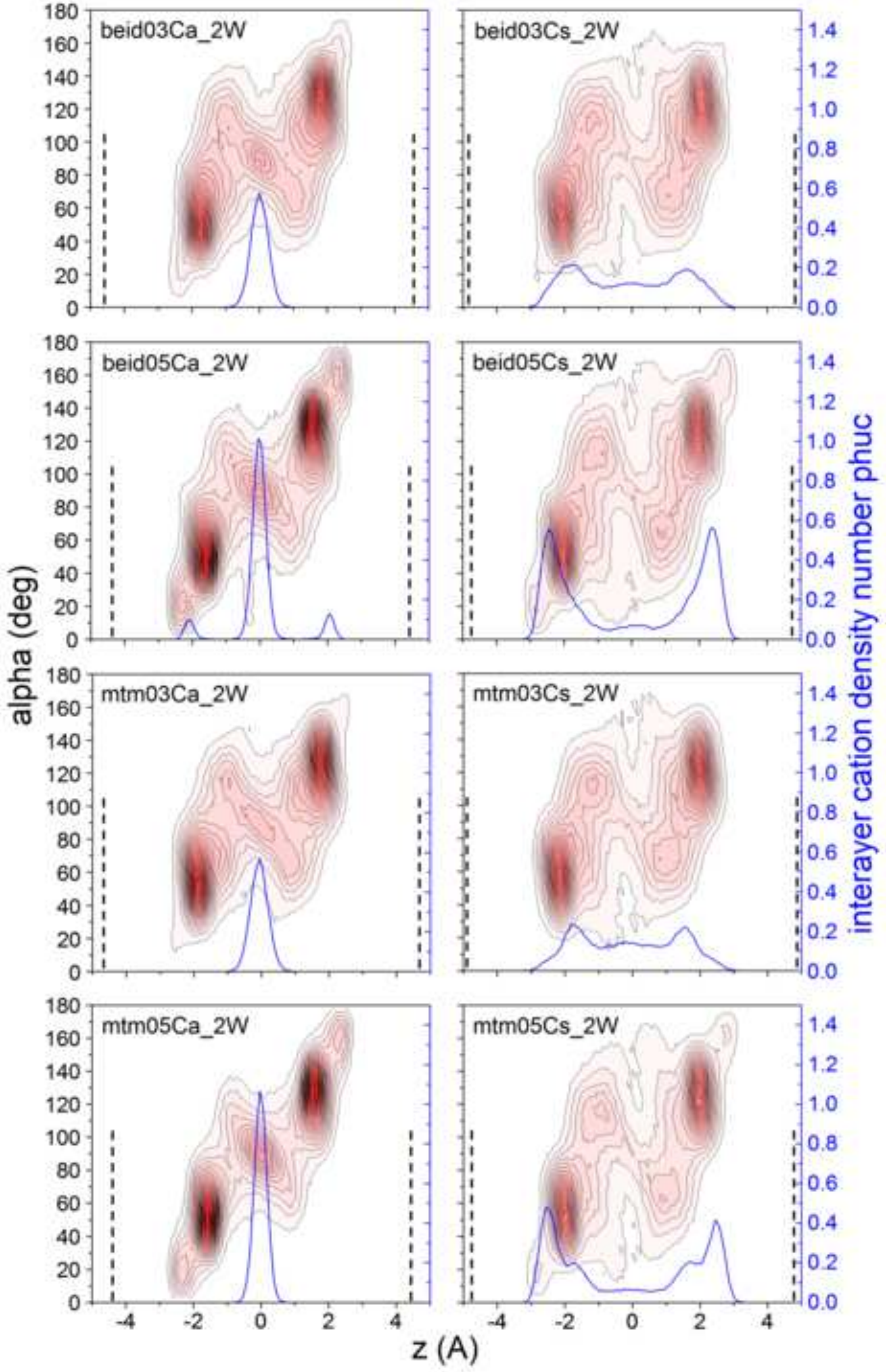
beid03Ca_2W
beid03Cs_2W
beid05Ca_2W
beid05Cs_2W
mtm03Ca_2W
mtm03Cs_2W
mtm05Ca_2W
mtm05Cs_2W
alpha (deg)
interayer cation density number phuc
z (A)
0
20
40
60
80
100
120
140
160
180
0.0
0.2
0.4
0.6
0.8
1.0
1.2
1.4
-4
-2
0
2
4

Figure_4

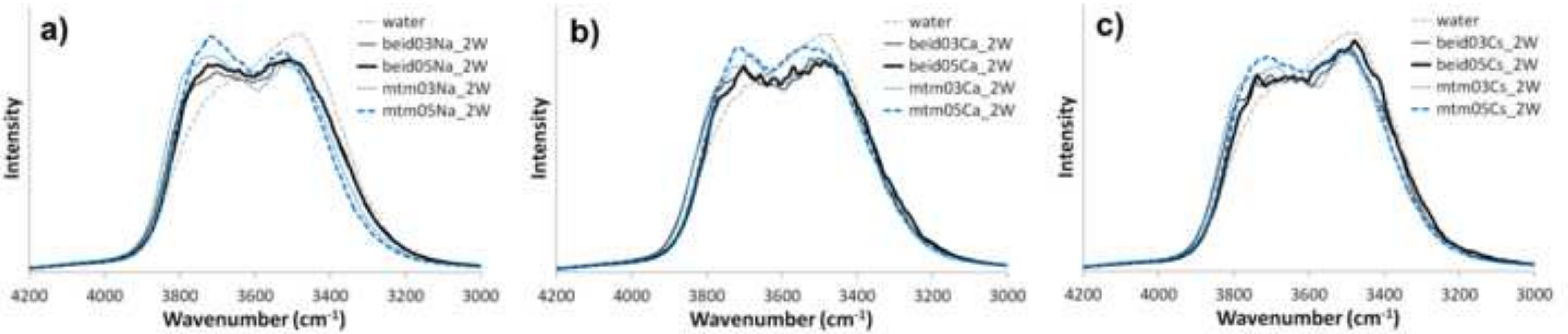
a)
water
beid03Na_2W
beid05Na_2W
mtm03Na_2W
mtm05Na_2W
Intensity
4200
4000
3800
3600
3400
3200
3000
Wavenumber (cm-1)
b)
water
beid03Ca_2W
beid05Ca_2W
mtm03Ca_2W
mtm05Ca_2W
Intensity
4200
4000
3800
3600
3400
3200
3000
Wavenumber (cm-1)
c)
water
beid03Cs_2W
beid05Cs_2W
mtm03Cs_2W
mtm05Cs_2W
Intensity
4200
4000
3800
3600
3400
3200
3000
Wavenumber (cm-1)

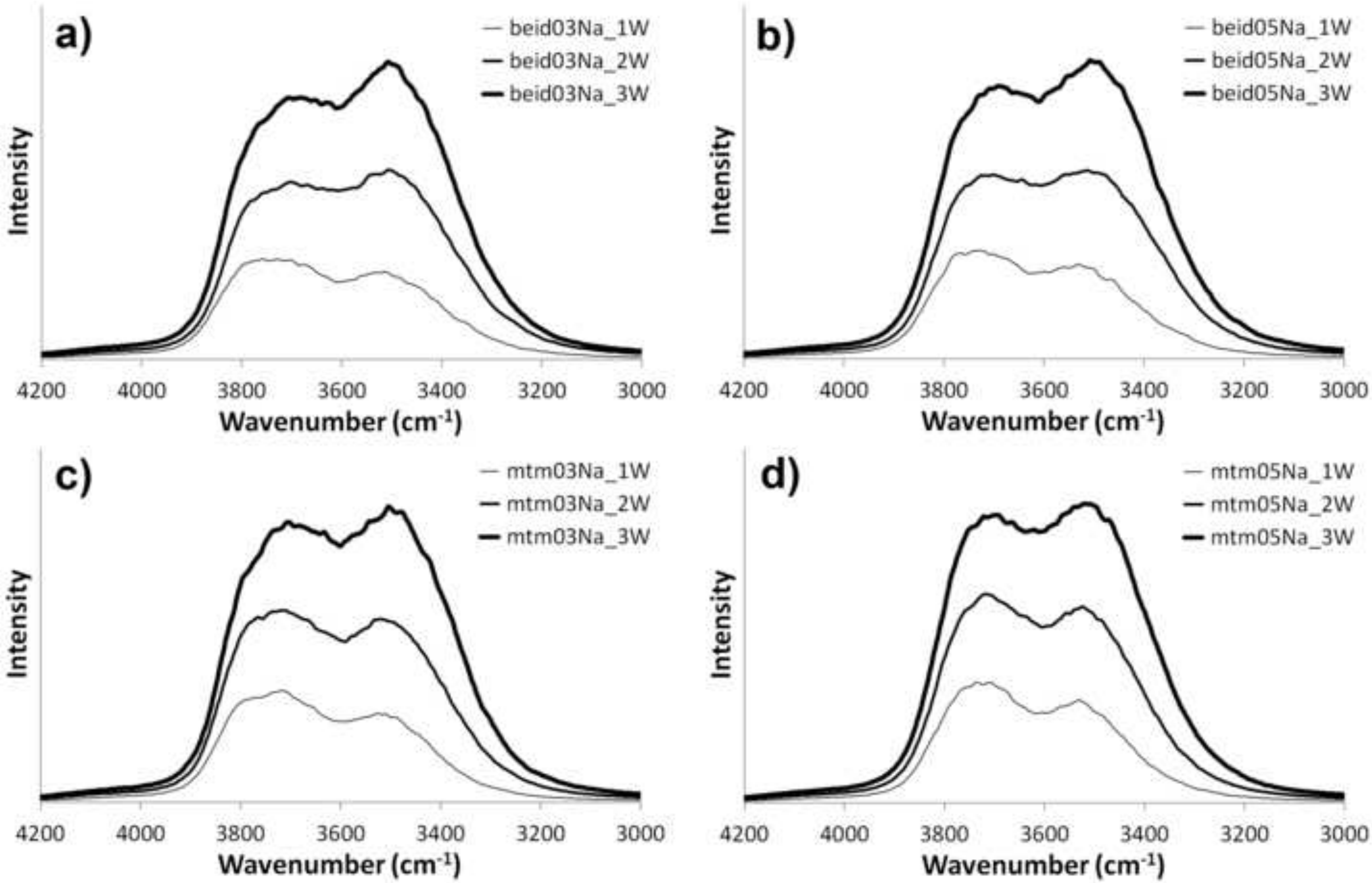
a)
beid03Na_1W
beid03Na_2W
beid03Na_3W
b)
beid05Na_1W
beid05Na_2W
beid05Na_3W
c)
mtm03Na_1W
mtm03Na_2W
mtm03Na_3W
d)
mtm05Na_1W
mtm05Na_2W
mtm05Na_3W
Intensity
4200
4000
3800
3600
3400
3200
3000
Wavenumber (cm-1)

Figure_6

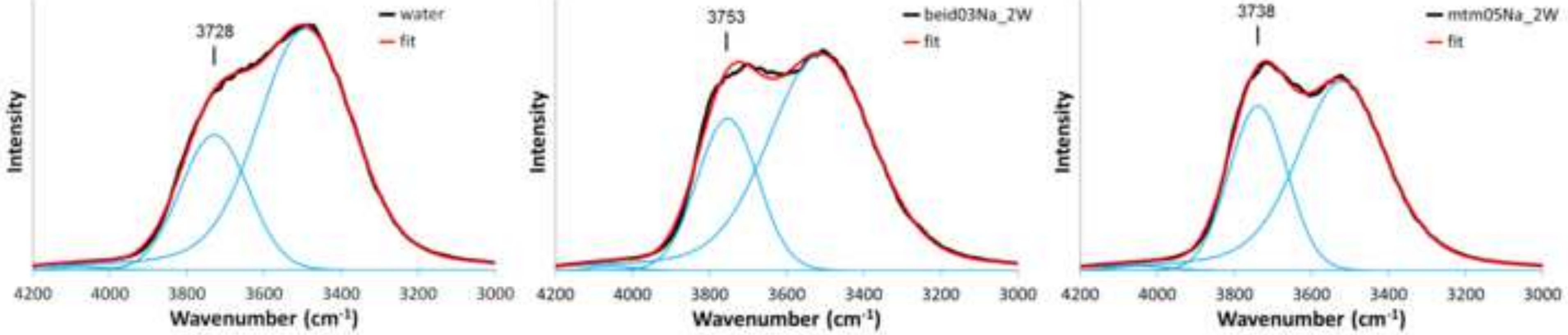
3728
water
fit
Intensity
4200
4000
3800
3600
3400
3200
3000
Wavenumber (cm⁻¹)
3753
beid03Na_2W
fit
Intensity
4200
4000
3800
3600
3400
3200
3000
Wavenumber (cm⁻¹)
3738
mtm05Na_2W
fit
Intensity
4200
4000
3800
3600
3400
3200
3000
Wavenumber (cm⁻¹)

Figure_7

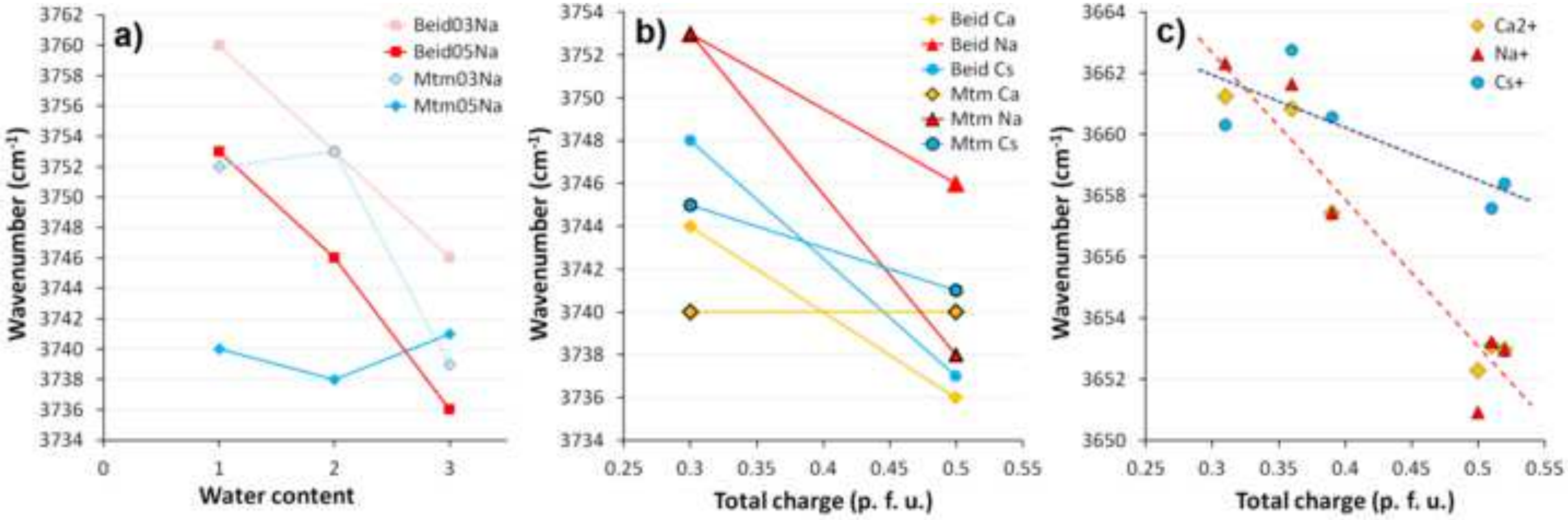
a)
Wavenumber (cm-1)
3734
3736
3738
3740
3742
3744
3746
3748
3750
3752
3754
3756
3758
3760
3762
0
1
2
3
Water content
Beid03Na
Beid05Na
Mtm03Na
Mtm05Na
b)
Wavenumber (cm-1)
3734
3736
3738
3740
3742
3744
3746
3748
3750
3752
3754
0.25
0.3
0.35
0.4
0.45
0.5
0.55
Total charge (p. f. u.)
Beid Ca
Beid Na
Beid Cs
Mtm Ca
Mtm Na
Mtm Cs
c)
Wavenumber (cm-1)
3650
3652
3654
3656
3658
3660
3662
3664
0.25
0.3
0.35
0.4
0.45
0.5
0.55
Total charge (p. f. u.)
Ca2+
Na+
Cs+

Figure_8

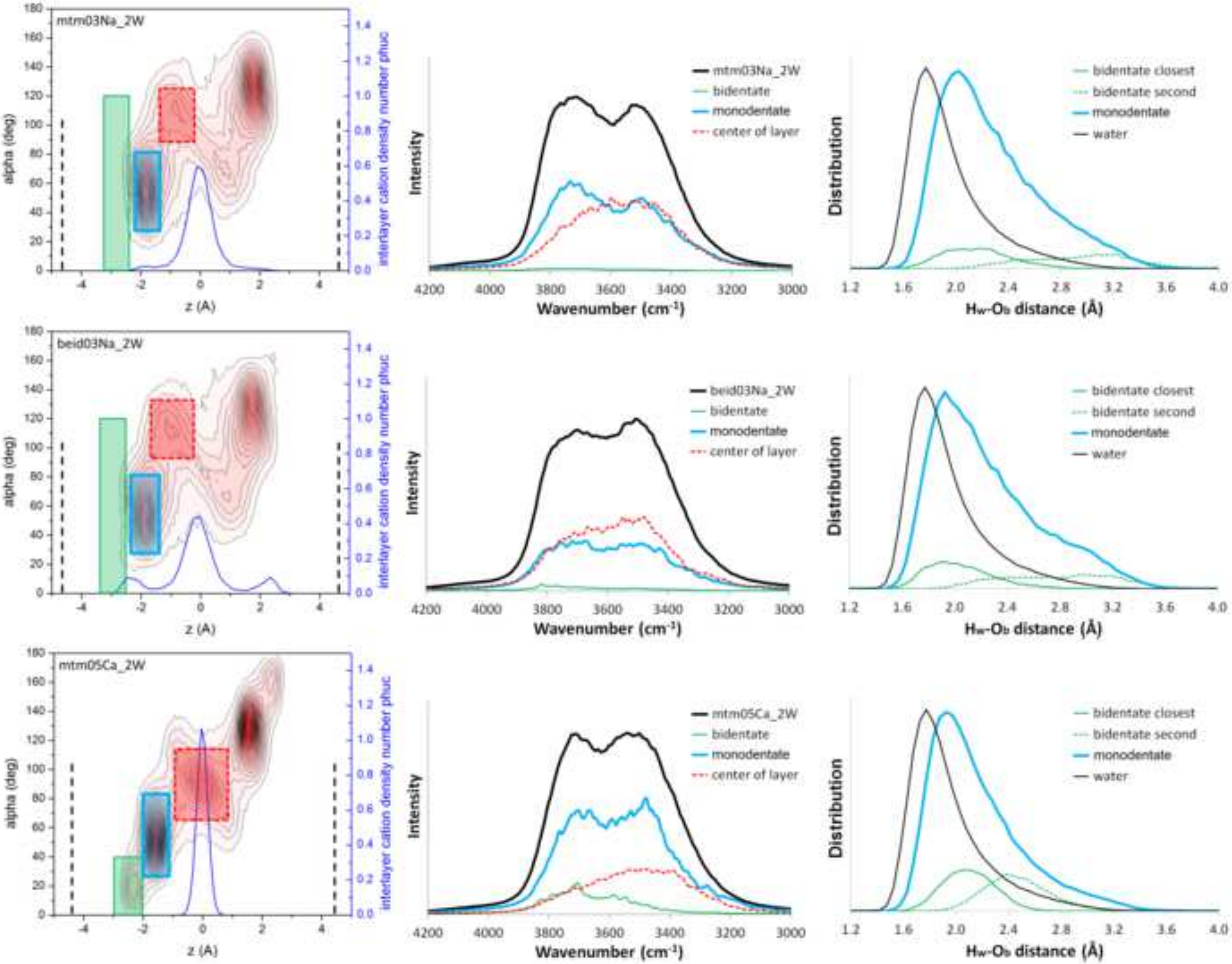
mtm03Na_2W
beid03Na_2W
mtm05Ca_2W
alpha (deg)
z (A)
interlayer cation density number phuc
Intensity
Wavenumber (cm⁻¹)
mtm03Na_2W
beid03Na_2W
mtm05Ca_2W
bidentate
monodentate
center of layer
Distribution
Hw-Ob distance (Å)
bidentate closest
bidentate second
monodentate
water

Figure_9

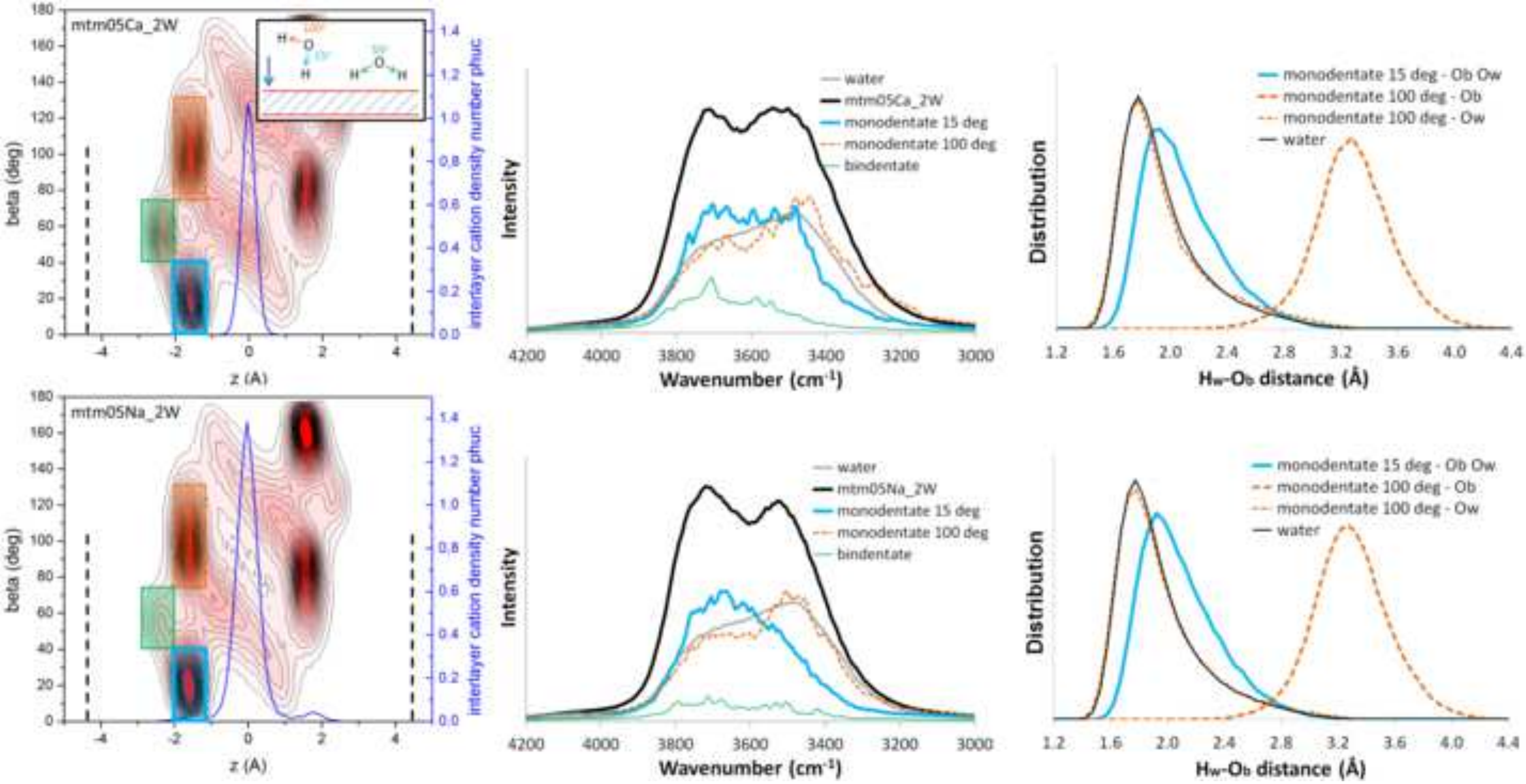
mtm05Ca_2W
beta (deg)
z (A)
interlayer cation density number phuc
Intensity
Wavenumber (cm⁻¹)
water
mtm05Ca_2W
monodentate 15 deg
monodentate 100 deg
bindentate
Distribution
Hw-Ob distance (Å)
monodentate 15 deg - Ob Ow
monodentate 100 deg - Ob
monodentate 100 deg - Ow
water
mtm05Na_2W
beta (deg)
z (A)
interlayer cation density number phuc
Intensity
Wavenumber (cm⁻¹)
water
mtm05Na_2W
monodentate 15 deg
monodentate 100 deg
bindentate
Distribution
Hw-Ob distance (Å)
monodentate 15 deg - Ob Ow
monodentate 100 deg - Ob
monodentate 100 deg - Ow
water
0
20
40
60
80
100
120
140
160
180
-4
-2
0
2
4
0.0
0.2
0.4
0.6
0.8
1.0
1.2
1.4
4200
4000
3800
3600
3400
3200
3000
1.2
1.6
2.0
2.4
2.8
3.2
3.6
4.0
4.4

Figure_10

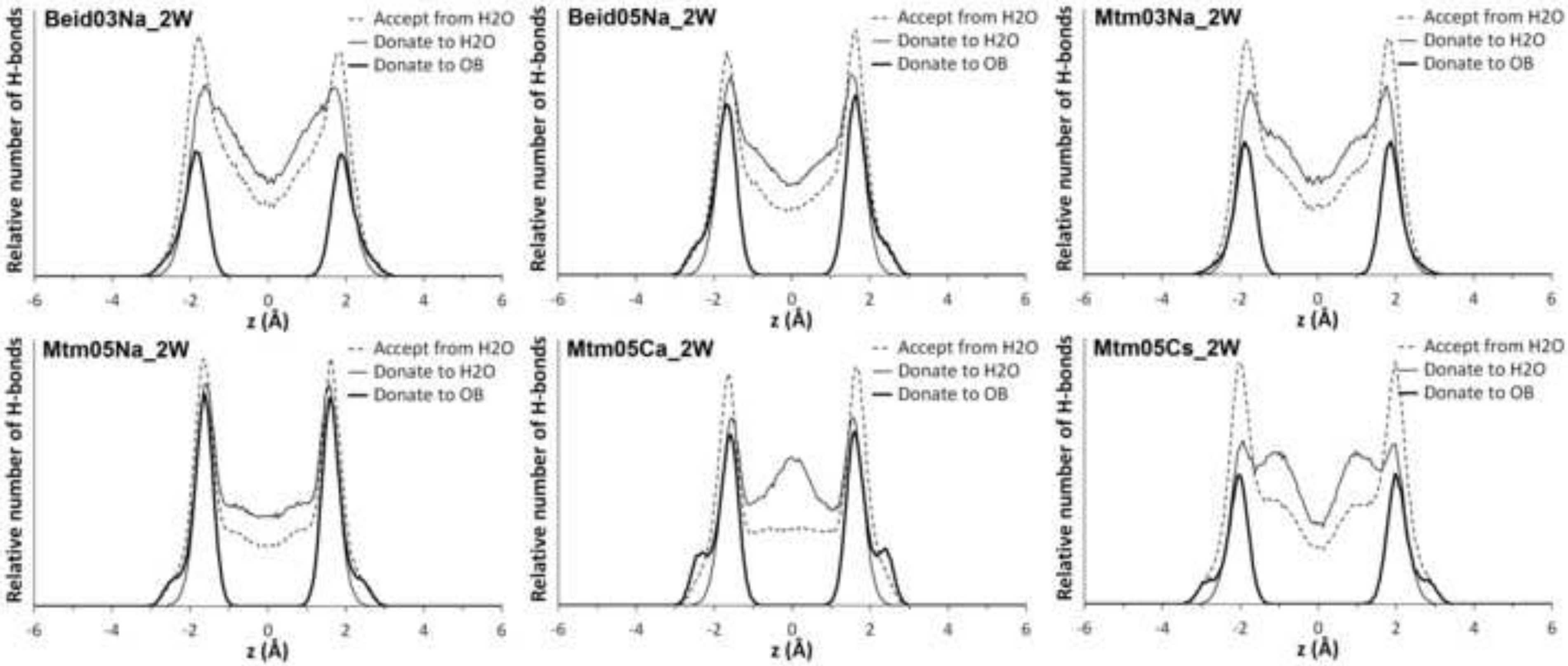
Beid03Na_2W
Beid05Na_2W
Mtm03Na_2W
Mtm05Na_2W
Mtm05Ca_2W
Mtm05Cs_2W
Accept from H2O
Donate to H2O
Donate to OB
Relative number of H-bonds
z (Å)
-6
-4
-2
0
2
4
6

Figure_11

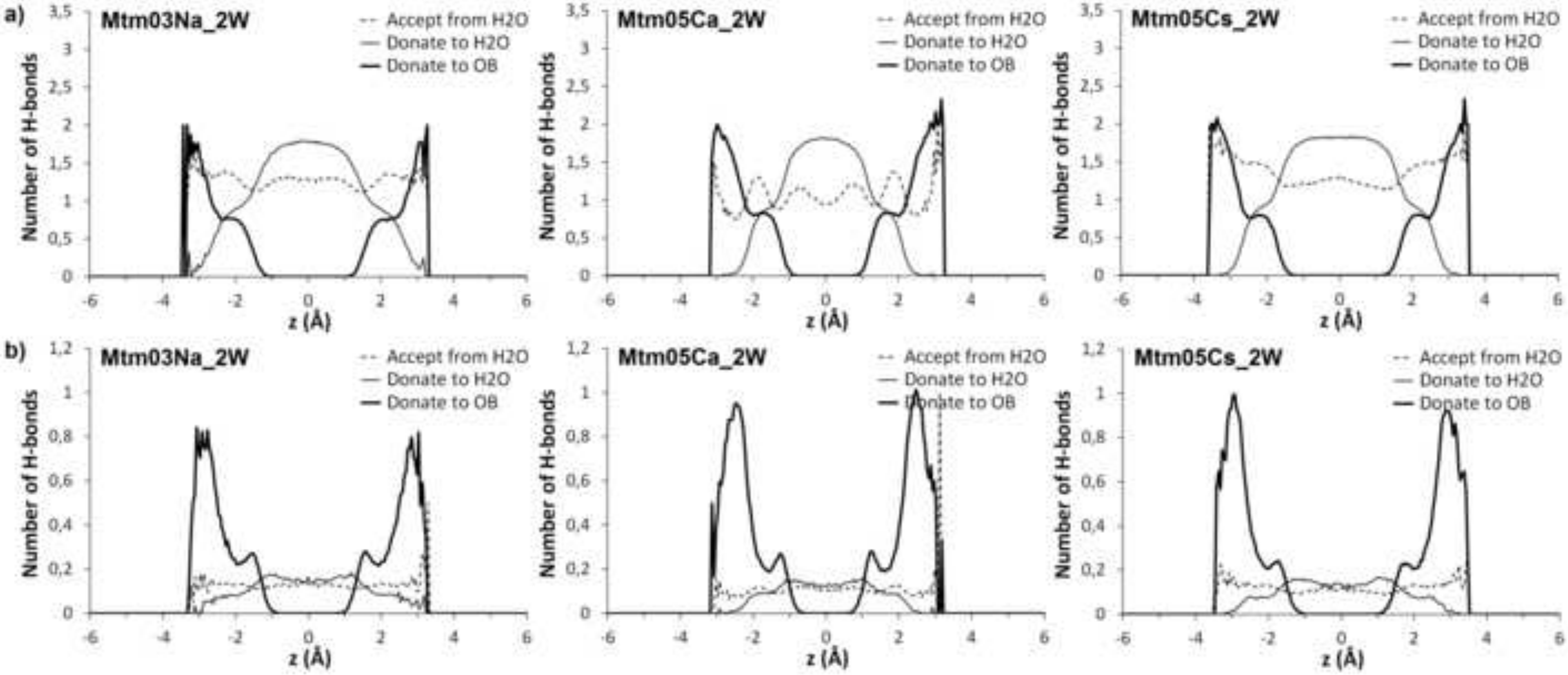
a)
b)
Mtm03Na_2W
Mtm05Ca_2W
Mtm05Cs_2W
Accept from H2O
Donate to H2O
Donate to OB
Number of H-bonds
z (Å)
3,5
3
2,5
2
1,5
1
0,5
0
1,2
1
0,8
0,6
0,4
0,2
-6
-4
-2
0
2
4
6